Bioorganic Chemistry 115 (2021) 105133

Contents lists available at ScienceDirect

Bioorganic Chemistry

journal homepage: www.elsevier.com/locate/bioorg

Novel thiomorpholine tethered isatin hydrazones as potential inhibitors of resistant *Mycobacterium tuberculosis*

Sivanandhan Karunanidhi [a], Balakumar Chandrasekaran [a], Rajshekhar Karpoormath [a,*], Harun M. Patel [a,b], Francis Kayamba [a], Srinivas Reddy Merugu [a], Vishal Kumar [a], Sanjeev Dhawan [a], Babita Kushwaha [a], Mavela Cleopus Mahlalela [a]

[a] Department of Pharmaceutical Chemistry, Discipline of Pharmaceutical Sciences, College of Health Sciences, University of KwaZulu-Natal (Westville), Durban 4000, South Africa

[b] R.C. Patel Institute of Pharmaceutical Education and Research, Shirpur (Dhule) 425405, Maharashtra, India

ARTICLE INFO

Keywords:
Synthesis
Multidrug-resistant tuberculosis
Isatin
Docking
MD simulations

ABSTRACT

Novel chemotherapeutic agents against multidrug resistant-tuberculosis (MDR-TB) are urgently needed at this juncture to save the life of TB-infected patients. In this work, we have synthesized and characterized novel isatin hydrazones 4(a-o) and their thiomorpholine tethered analogues 5(a-o). All the synthesized compounds were initially screened for their anti-mycobacterial activity against the $H_{37}Rv$ strain of *Mycobacterium tuberculosis* (MTB) under level-I testing. Remarkably, five compounds 4f, 4h, 4n, 5f and 5m (IC_{50} = 1.9 μM to 9.8 μM) were found to be most active, with 4f (IC_{50} = 1.9 μM) indicating highest inhibition of $H_{37}Rv$. These compounds were further evaluated at level-II testing against the five drug-resistant strains such as isoniazid-resistant strains (INH-R1 and INH-R2), rifampicin-resistant strains (RIF-R1 and RIF-R2) and fluoroquinolone-resistant strain (FQ-R1) of MTB. Interestingly, 4f and 5f emerged as the most potent compounds with IC_{50} of 3.6 μM and 1.9 μM against RIF-R1 MTB strain, followed by INH-R1 MTB strain with IC_{50} of 3.5 μM and 3.4 μM, respectively. Against FQ-R1 MTB strain, the lead compounds 4f and 5f displayed excellent inhibition at IC_{50} 5.9 μM and 4.9 μM, respectively indicating broad-spectrum of activity. Further, molecular docking, ADME pharmacokinetic and molecular dynamics simulations of the compounds were performed against the DNA gyrase B and obtained encouraging results.

1. Introduction

Tuberculosis (TB), a communicable disease mainly caused by a single infectious microorganism *Mycobacterium tuberculosis* (MTB), and is known for one of the top 10 causes of death worldwide [1]. A recent global report (2019) on tuberculosis by world health organization (WHO) documented about 1.5 million deaths among 10 million cases of TB that clearly alarming the severity of this deadly disease [1]. Moreover, a syndemic interaction between acquired immuno deficiency syndrome (AIDS) and TB has become an epidemic, since 20% of the deaths are due to co-infection of TB in HIV-positive patients. Current treatment of TB composed of initial two months of intensive stage therapy with four important first-line oral anti-TB drugs (isoniazid, rifampicin, pyrazinamide and ethambutol) followed by four months of continuation stage management with the administration of isoniazid and rifampicin [2]. However, poor patient compliance owing to long-term treatment regimen and lack of new broad spectrum, potent anti-mycobacterial drugs has greatly contributed to the spontaneous emergence of drug-resistant TB such as multidrug-resistant TB (MTR-TB; refers to the resistant against isoniazid and rifampicin) and extremely drug resistant TB (XDR-TB; a MDR-TB with resistance towards fluoroquinolones and/or any second-line anti-TB drugs) [3]. Steady rise in MDR-TB and XDR-TB, especially in developing countries has further complicated the treatment and management of TB, causing serious health and socio-economic concerns. In addition to the existing challenges, recent emergence of totally drug resistant TB (TDR-TB; resistant against all currently available anti-TB drugs) [4,5] has become a greatest threat to human kind. It is also very important to note that there are no new drugs introduced into the market for the treatment of MDR/XDR-TB for the past four decades except Bedaquiline, which got provisional

* Corresponding author.
E-mail addresses: karpoormath@ukzn.ac.za, rvk2006@gmail.com (R. Karpoormath).

https://doi.org/10.1016/j.bioorg.2021.105133
Received 23 May 2021; Received in revised form 22 June 2021; Accepted 26 June 2021
Available online 3 July 2021

approval in the year 2012 by US-FDA [6]. This is the latest development in the current TB management and this scenario indicates that there is an urgent need to discover novel drug scaffolds which can resolve the drug resistance problems with broad-spectrum of activity, and devoid of serious side effects.

Structure-based drug design (SBDD) is one of the successful approaches in the new drug discovery involving the use of 3D structures of the target proteins [7-9]. DNA gyrase including *Mycobacterium* species is a tetrameric holoenzyme with two A (GyrA) and two B (GyrB) subunits that are responsible for maintaining the topology of the DNA duplex during the replication process. GyrA subunit involved in the breakage and reunion of the DNA, whereas the GyrB subunit exhibits an ATP-ase activity. In the absence of ATP, the DNA gyrase enzyme catalyzes only to the relaxation of the supercoiled DNA. DNA gyrase inhibition using fluoroquinolone antibiotics is a clinically validated therapeutic approach to treat drug-resistant bacterial infections [10]. MTB DNA gyrase has recently attracted greater attention as potential drug target for the new generation of anti-TB drugs to combat MDR-TB, and fluoroquinolone-resistant MTB. There are at least two types of gyrase inhibitors reported in the literature with potent activity against MTB [11-13] such as fluoroquinolones and aminopiperidines as GyrA inhibitors, while aminopyrazinamides, thiazolopyridine ureas, aminobenz-imidazoles and pyrrolamides reported as GyrB inhibitors [14]. GyrB is the primary target for clinically important drug Novobiocin, the only approved GyrB inhibitor [15]. In 2013, the co-crystallized DNA GyrB ATPase protein (PDB ID: 4B6C) with bound inhibitor (aminopyrazinamide) was reported, which paved the way to understand the structural interactions at the DNA GyrB active-site for the discovery of novel anti-TB agents [16].

It is well documented in literature that isatin (1*H*-indole-2,3-dione) is one of the versatile building block or scaffolds in medicinal chemistry due to its wide range of pharmacological activities including anti-viral [17], anti-angiogenic [18], anti-cancer [19], anti-malarial [20], anti-microbials [21,22]. In particular, tryptanthrin (**I**) (Fig. 1), an isatin hybridized natural product reported as a potent anti-mycobacterial agent [23]. Feng et al., documented that isatin tethered balofloxacin exhibited improved anti-mycobacterial activity against $H_{37}Rv$ than balofloxacin alone [24]. In the subsequent year, the same research group [25] reported a higher inhibitory activity for the ciprofloxacin tethered isatin hybrid. Sriram et. al., [26] demonstrated Gatifloxacin hybridized isatin (**II**) as promising anti-mycobacterial compound with MTB DNA gyrase inhibition (Fig. 1). Furthermore, several isatin hybrids (**III-VI**) have displayed the encouraging anti-mycobacterial activity profiles [27-30] (Fig. 1).

Hydrazone, a bioactive linker is found mostly in the heterocyclic medicinal compounds. Sriram et al., [31] investigated the anti-mycobacterial activity of isonicotinyl hydrazones and reported potent inhibition against MTB $H_{37}Rv$ strain. Küçükgüzel et al., [32] also identified some hydrazone derivatives as effective anti-mycobacterial compounds. Similarly, a momentous candidate, thiomorpholine can improve the anti-mycobacterial activity of heterocyclic compounds through a synergistic effect. Sutezolid (**VI**), a thiomorpholine containing anti-mycobacterial compound (Fig. 1) is presently under the clinical development as a drug candidate for the treatment of XDR-TB [33]. These inspiring investigations and in continuation of our research towards the discovery of novel anti-mycobacterial agents [34-36], we envisaged to design, synthesize and evaluate potential anti-mycobacterial activities of novel isatin-based analogues.

2. Results and discussion

2.1. Chemistry

The synthesis of the final thiomorpholine tethered isatin hydrazones was achieved in higher yield through a facile and straightforward three step reactions employing a microwave reactor (CEM Discover, Explorer-12 Hybrid, Microwave conditions: 80 °C at 150 psi) except for the final step. Indoline-2,3-dione [isatin; **1a**] or 5-chloro-indoline-2,3-dione [5-chloro-isatin; **1b**] was treated individually with hydrazine hydrate (50–60%) in methanol to yield respective 3-hydrazonoindoline-2-ones (**2a** and **2b**) *via* a simple condensation reaction [37,38]. Under microwave irradiation, the free primary amino group present in **2a** or **2b** reacted with various aldehydes (**3**) in acidic medium to form respective Schiff-bases **4(a-o)** in good yields [39,40]. The tethering of

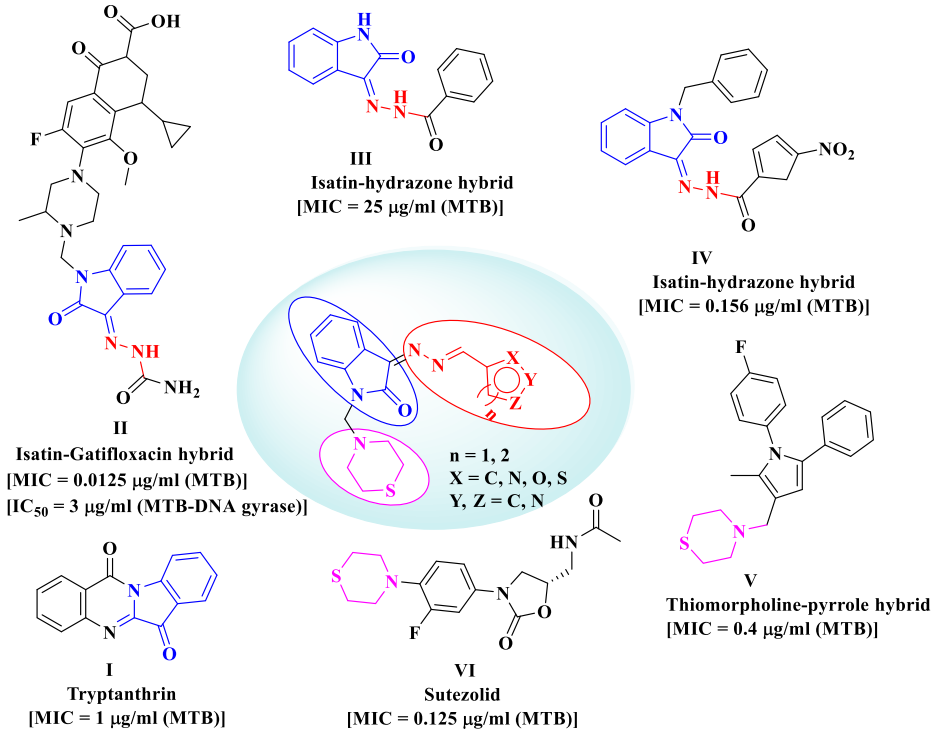

Fig. 1. Literature reported anti-mycobacterial agents to design of novel isatin hybrids.

thiomorpholine to **4(a-o)** was achieved using 34% formaldehyde as a source of methylene (–CH_2) linker in ethanol, yielding the final target compounds **5(a-o)**, quantitatively (Scheme 1).

The expected structures of the isatin hydrazones **4(a-o)** and the thiomorpholine tethered final compounds **5(a-o)** were confirmed based on their spectral data. In FT-IR spectra, the appearance of the vibrational bands around 1510 cm^{-1} for N—H bending, 1597 cm^{-1} (C═O stretch), 1714 cm^{-1} (C═N stretch), and 3133 cm^{-1} for N—H stretching supported the formation of compounds **4(a-o)**. This was further substantiated from the ^{1}H NMR spectra, wherein a distinctive singlet peak resonating around δ 8.37 ppm to δ 8.94 ppm was attributed to the Schiff base proton (-N = C<u>H</u>–) and isatin-NH appeared as singlet between δ 10.09 ppm and δ 11.02 ppm, respectively confirming the formation of **4(a-o)**. Apart from aromatic or heterocyclic carbon signals, the ^{13}C NMR spectra displayed a characteristic carbon signal of Schiff base carbon (-N = <u>C</u>H–) between δ 152 ppm to δ 162 ppm, validating the formation of compounds **4(a-o)**.

The absence of the singlet signal corresponding to N—H proton of isatin moiety and appearance of new methylene (–C<u>H</u>$_2$–) signal at δ 4.49 ppm in ^{1}H NMR spectra of **5(a-o)** confirmed the anticipated structures of final compounds. Further, new triplet signal in the aliphatic region around δ 2.58 ppm, thiomorpholine protons at δ 2.84 ppm and the most characteristic Schiff base protons (-N = C<u>H</u>–) resonating between δ 8.51 ppm and δ 9.01 ppm authenticated the formation of **5(a-o)**. This has been further characterized by ^{13}C NMR of **5(a-o)** which demonstrated the significant methylene carbon (–<u>C</u>H$_2$–) signal appeared in the range of δ 62.06 ppm to δ 62.79 ppm and the presence of carbon signals (δ 26.93 ppm and δ 55.73 ppm) corresponding to the thiomorpholine moiety. In addition, the respective accurate mass signals displayed by the HRMS data confirmed the formation of final compounds **5(a-o)**, which revealed the positive correlation with the expected molecular weights. All the spectral images (FT-IR, ^{1}H NMR, ^{13}C NMR and representative HRMS) of the compounds are provided in the supporting information.

2.2. Biological studies

2.2.1. Anti-mycobacterial studies under Level-I (MTB $H_{37}Rv$) evaluation

In vitro anti-mycobacterial evaluation of all the newly synthesized intermediates **4(a-o)** and the final compounds **5(a-o)** was carried out at Infectious Disease Research Institute (IDRI) within the National Institute of Allergy and Infectious Diseases (NIAID) screening program (Bethesda, MD, USA). The minimum inhibitory concentration (MIC) was determined against *M. tuberculosis* strain $H_{37}Rv$ grown under aerobic conditions by using a dual read-out (OD590 and fluorescence) assay protocol [41,42]. All the synthesized compounds exhibited significant anti-mycobacterial activity profile against the tested MTB $H_{37}Rv$ strain under level-I screening program (Table 1). Remarkably, 5-nitro-thiophene substituted hybrid **4f** presented highest potency against MTB $H_{37}Rv$ strain with a promising IC_{50} value of 1.9 μM and MIC at 2.3 μM. A couple of other compounds, **4h** bearing 5-nitro-furyl substitution and the bioisosteric pair **4n** containing 5-nitro-thiophene substituent, exhibited relatively higher MTB $H_{37}Rv$ inhibition with IC_{50} values 7.6 μM and 9.8 μM, respectively. Further, **4h** and **4n** demonstrated impressive MIC values at 12 μM and 17 μM, respectively indicating their encouraging anti-mycobacterial potency. The unsubstituted thiophene hybridized compound **4d** revealed a moderate inhibition with IC_{50} value of 56 μM. Remaining compounds in this series bearing other substitutions such as aromatic or six-membered heterocyclic rings were found to be poor or moderately active. It was observed that compounds having 5-nitro-thiophene/furyl substitutions indicated best activity against the MTB $H_{37}Rv$ strain.

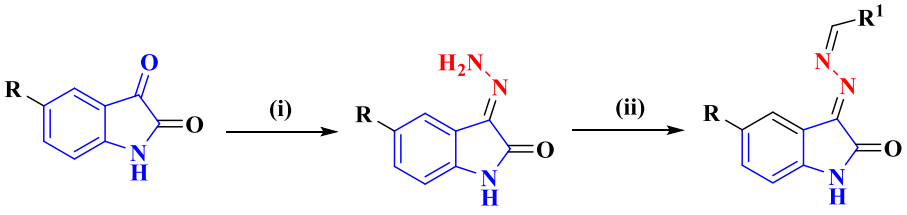

1a, R = H,
1b, R = Cl

2(a,b)

4(a-o)

4a, 5a; R=H, R^1= 4-methoxyphenyl
4b, 5b; R=H, R^1= 3,4-dimethoxyphenyl
4c, 5c; R=H, R^1= 3-pyridinyl
4d, 5d; R=H, R^1= 2-thienyl
4e, 5e; R=H, R^1= 2-furyl
4f, 5f; R=H, R^1= 5-nitro-2-thienyl
4g, 5g; R=H, R^1= 4-pyridinyl
4h, 5h; R=H, R^1= 5-nitro-2-furyl
4i, 5i; R=Cl, R^1= 4-methoxyphenyl
4j, 5j; R=Cl, R^1= 3,4-dimethoxyphenyl
4k, 5k; R=Cl, R^1= 3-pyridinyl
4l, 5l; R=Cl, R^1= 2-thienyl
4m, 5m; R=Cl, R^1= 2-furyl
4n, 5n; R=Cl, R^1= 5-nitro-2-thienyl
4o, 5o; R=Cl, R^1= 4-pyridinyl

5(a-o)

Scheme 1. Synthesis of thiomorpholine tethered isatin hydrazones. Reagents and conditions: (i) Hydrazine hydrate, methanol, microwave irradiation, 80 °C, 2 mins, 150 psi; (ii) Substituted aromatic/heteroaromatic aldehydes (**3**), ethanol, microwave irradiation, 80 °C, 10 mins, 150 psi; (iii) Thiomorpholine, formaldehyde, ethanol, stir, RT, 2 h.

Table 1
Anti-mycobacterial activity data of the synthesized compounds **4(a-o)** and **5(a-o)**.

Compound	*M. tuberculosis* [a] ($H_{37}Rv$)			Compound	*M. tuberculosis* [a] ($H_{37}Rv$)			Compound	*M. tuberculosis* [a] ($H_{37}Rv$)		
	MIC	IC_{50}	IC_{90}		MIC	IC_{50}	IC_{90}		MIC	IC_{50}	IC_{90}
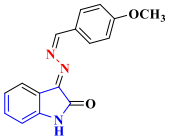 **4a**	>200	>100	>100	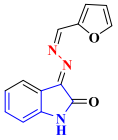 **4e**	>200	101	>200	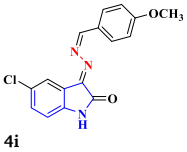 **4i**	>200	50	50
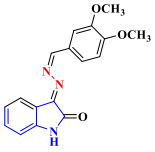 **4b**	>100	29	60	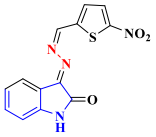 **4f**	2.3	1.9	3.4	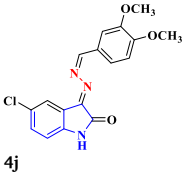 **4j**	>100	>100	>100
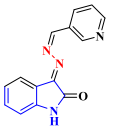 **4c**	>200	113	>200	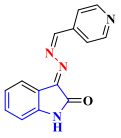 **4g**	>200	92	>200	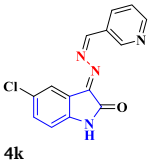 **4k**	180	65.4	135
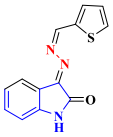 **4d**	88	56	56	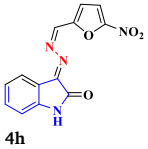 **4h**	12	7.6	10	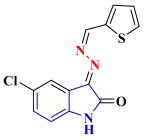 **4l**	>200	>50	>50

Compound	*M. tuberculosis* [a] ($H_{37}Rv$)			Compound	*M. tuberculosis* [a] ($H_{37}Rv$)			Compound	*M. tuberculosis* [a] ($H_{37}Rv$)		
	MIC	IC_{50}	IC_{90}		MIC	IC_{50}	IC_{90}		MIC	IC_{50}	IC_{90}
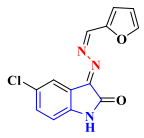 *4m*	>200	132	>200	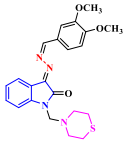 **5b**	>200	190	>200	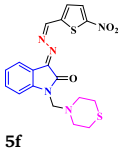 **5f**	7.0	3.9	6.9
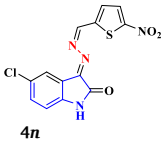 ***4n***	17	9.8	17	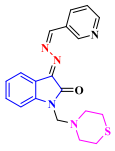 **5c**	>200	140	>200	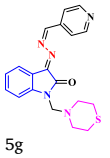 5g	>200	66	150
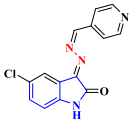 4o	>200	190	>200	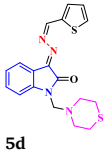 **5d**	81	32	75	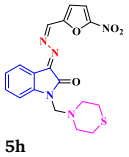 **5h**	9.0	6.4	8.4
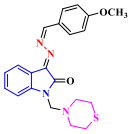 **5a**	>200	95	>200	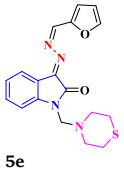 **5e**	>200	120	>200	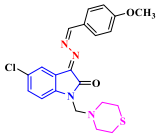 **5i**	>200	190	>200

Compound	*M. tuberculosis* [a] ($H_{37}Rv$)			Compound	*M. tuberculosis* [a] ($H_{37}Rv$)			Compound	*M. tuberculosis* [a] ($H_{37}Rv$)		
	MIC	IC_{50}	IC_{90}		MIC	IC_{50}	IC_{90}		MIC	IC_{50}	IC_{90}
	>200	190	>200		5.6	3.9	4.7	Std[b]	0.0067	–	–

(*continued on next page*)

Table 1 (*continued*)

Compound	*M. tuberculosis* [a] ($H_{37}Rv$)			Compound	*M. tuberculosis* [a] ($H_{37}Rv$)			Compound	*M. tuberculosis* [a] ($H_{37}Rv$)		
	MIC	IC_{50}	IC_{90}		MIC	IC_{50}	IC_{90}		MIC	IC_{50}	IC_{90}
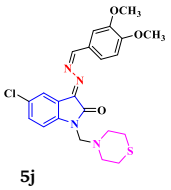 **5j**	>200	100	>200	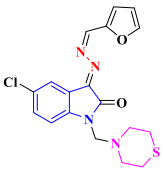 **5*m***	37	23	34				
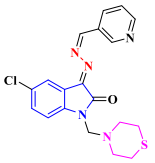 **5k**	>200	190	>200	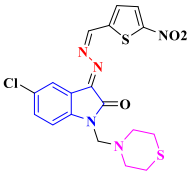 **5*n***	87	47	77				
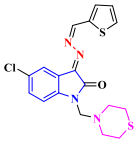 **5l**				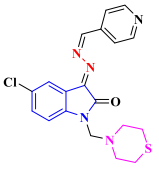 **5o**							

[a] Concentration in μM.
[b] Std is Rifampicin.

Recent literature reports indicated that thiomorpholine moiety enhanced the antimicrobial and mycobacterial potency through synergistic effect [29,43]. To further improve the anti-mycobacterial potency of **4(a-o)** series, we envisaged to incorporate thiomorpholine moiety to isatin—N—H *via* a lipophilic methylene (–CH_2) linker, resulting in a series of novel compounds **5(a-o)**. The anti-mycobacterial screening results of **5(a-o)** revealed compound **5f** with the best inhibition against MTB $H_{37}Rv$ strain with IC_{50} value of 3.9 μM and MIC of 7.0 μM. However, it was observed that the activity of compound **5f** was quite lower than **4f**. Interestingly, both **4f** and **5f** had one common feature that is 5-nitro-thiophenyl substitution in their structures which contributed positively and substantiating the role of electron-withdrawing nitro group on π-excessive 5-membered heterocyclic system towards the accomplishment of higher anti-mycobacterial potency. An equipotent compound **5 m** containing unsubstituted furyl ring displayed IC_{50} value of 3.9 μM and MIC of 5.6 μM, respectively. Bioisosteric replacement of the unsubstituted furyl in compound **5 m** with 5-nitro substituted furyl ring resulted the compound **5 h** with one-fold lower anti-mycobacterial activity (IC_{50} = 6.4 μM). Though the compound **5n** had 5-nitro-thiophenyl substitution on the chloroisatin scaffold, it could only to show a moderate inhibition at IC_{50} 23 μM. Similarly, compound **5o** (IC_{50} = 47 μM) with pyridine substituent displayed no significant activity, which could be attributed to the π-deficient pyridine system for the reduced potency. All the remaining compounds in this series displayed little or no anti-mycobacterial activity. Level-1 anti-mycobacterial screening of the thirty compounds led to the identification of five most active compounds, which were considered for further assessment for level-II anti-mycobacterial screening against drug-resistant MTB strains.

2.2.2. *Anti-mycobacterial studies under Level-II (Drug-resistant MTB strains) evaluation*

With an encouraging anti-mycobacterial result from level-I screening, five most active compounds **4f**, **4h**, **4n**, **5f** and **5m** were further considered for level-II screening to evaluate their efficacy under different circumstances such as varied oxygen conditions, activity against multidrug-resistant mycobacterial isolates and other strains of mycobacterial species. In level-II testing, these five compounds were initially evaluated against five drug-resistant isolates namely INH-R1, INH-R2, RIF-R1, RIF-R2, and FQ-R1 of MTB under aerobic conditions. The results of level-II testing data indicated once again that compounds **4f** and **5f** presented considerable activity against all the tested drug-resistant strains (Table 2), which was followed by **4n** and **5m**. Unambiguously, the thiomorpholine-tethered analogue **5f** exhibited an interesting and potent inhibition of rifampicin resistant R1 (RIF-R1) strain with an IC_{50} of 1.9 μM that is nearly equal to the standard drug rifampicin (IC_{50} = 1.2 μM). Against RIF-R2 strain, **5f** demonstrated higher potency (IC_{50} = 8.4 μM) than the rifampicin (IC_{50} > 50 μM) indicating the potential anti-TB activity against rifampicin-resistant MTB strains. Importantly, **5f** showed higher inhibition with IC_{50} 3.4 μM (against INH-R1 strain) and 5.3 μM (against INH-R2 strain) than the standard drug isoniazid (IC_{50} > 200 μM) which authenticated for their prospective use in INH-resistant TB therapy. Furthermore, **5f** displayed higher inhibition of FQ-R1 strain with the promising IC_{50} of 4.9 μM which is considerably potent than the standard drug levofloxacin (IC_{50} = 12 μM) indicating **5f** could be a lead compound effective against XDR-TB. Investigation of SAR of the corresponding intermediate **4f** designated a moderate inhibition against rifampicin resistant R1 (RIF-R1) strain with an IC_{50} of 3.6 μM, a two-fold lower activity compared to **5f**. Remarkably, **4f** demonstrated 10-fold higher potency (IC_{50} = 5.3 μM) than the standard reference rifampicin (IC_{50} > 50 μM) against RIF-R2 strain. The same compound **4f** demonstrated equipotent anti-TB activity (IC_{50} = 3.5 μM) as compared to **5f** against INH-R1 strain. Against INH-R2 strain, **4f** presented an outstanding inhibition (IC_{50} = 4.6 μM) than the standard drug isoniazid (IC_{50} > 200 μM) which validated its anti-TB potential. Moreover, **4f** exhibited two-fold higher inhibition of FQ-R1 strain (IC_{50} = 5.9 μM) than the standard drug levofloxacin (IC_{50} = 12 μM) thereby signifying the intermediate **4f** could be effective against XDR-TB strain. Thus, this work resulted in the discovery of two promising leads **4f** and **5f** as highly potent anti-mycobacterial compounds, which can be further optimized as potential inhibitors of MDR- and XDR-resistant MTB strains (Fig. 2).

Table 2
Anti-mycobacterial activity data of selected compounds against five drug-resistant isolates of *M. tuberculosis*.

Compound	INH-R1[a]			INH-R2[b]			RIF-R1[c]			RIF-R2[d]			FQ-R1[e]		
	MIC (μM)	IC_{50} (μM)	IC_{90} (μM)	MIC (μM)	IC_{50} (μM)	IC_{90} (μM)	MIC (μM)	IC_{50} (μM)	IC_{90} (μM)	MIC (μM)	IC_{50} (μM)	IC_{90} (μM)	MIC (μM)	IC_{50} (μM)	IC_{90} (μM)
4f	**5.0**	**3.5**	**4.4**	**8.6**	**4.6**	**11**	**7.5**	**3.6**	**7.7**	**19**	**5.3**	**24**	**20**	**5.9**	**21**
4h	21	16	21	21	14	17	9.2	4.4	11	31	25	27	35	22	41
4n	22	14	16	43	24	43	20	7.7	24	56	24	59	130	28	>100
5f	**5.5**	**3.4**	**5.9**	**14**	**5.3**	**16**	**9.6**	**1.9**	**14**	**17**	**8.4**	**18**	**16**	**4.9**	**23**
5m	42	26	29	28	20	28	24	11	25	38	25	39	44	27	32
Rifampicin	0.018	0.0084	0.022	0.0065	0.0047	0.012	2	1.2	2.3	>50	>50	>50	0.027	0.013	0.039
Isoniazid	>200	>200	>200	>200	>200	>200	0.17	0.15	0.21	0.62	0.54	0.6	0.35	0.36	0.47
Levofloxacin	1.2	0.64	1.4	1.4	0.84	1.4	0.76	0.59	0.91	1.1	0.6	1.2	20	12	22

[a] INH-R1 was derived from $H_{37}Rv$ and is a katG mutant (Y155* = truncation).
[b] INH-R2 is strain ATCC35822.
[c] RIF-R1 was derived from H37Rv and is a nrpoB mutant (S522L).
[d] RIF-R2 is strain ATCC35828.
[e] FQ-R1 is a fluoroquinolone-resistant strain derived from $H_{37}Rv$ and is a gyrB mutant (D94N). INH, isoniazid; RIF, rifampicin; FQ, Fluoroquinolone.

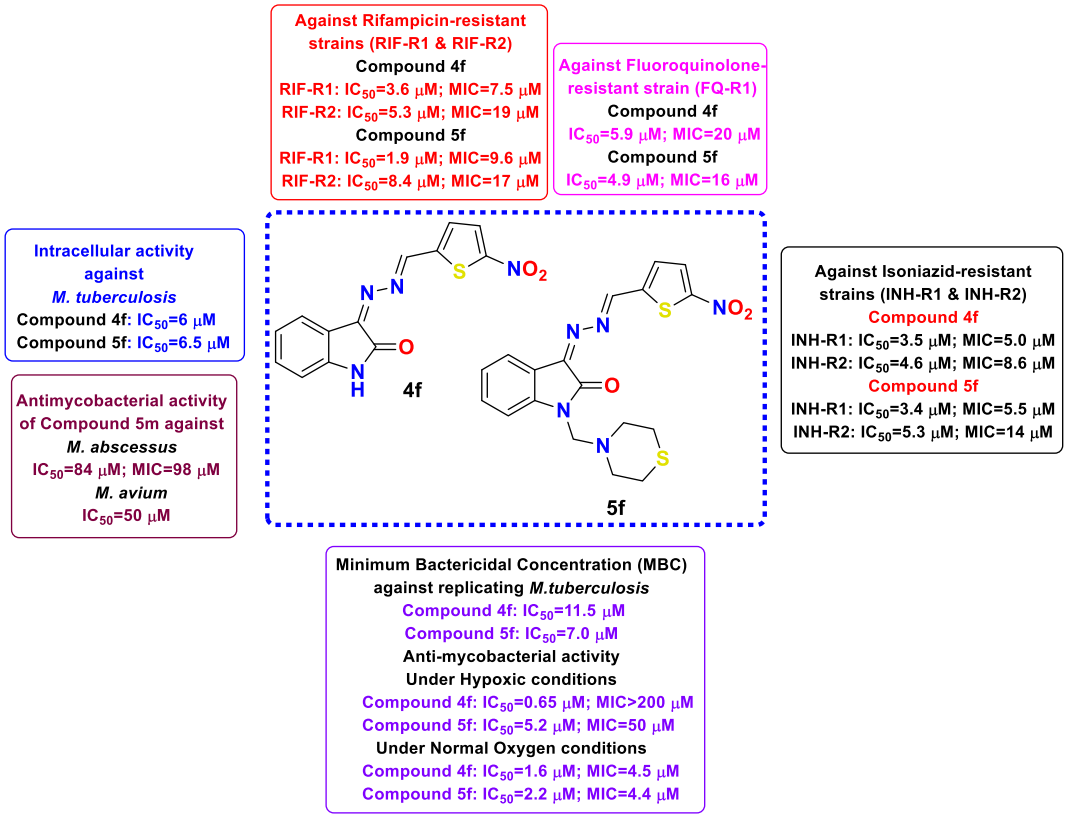

Fig. 2. Anti-mycobacterial activity of the most active compounds **4f** and **5f**.

2.2.3. *MIC assay under hypoxic (low) oxygen condition and MBC determination*

The promising five compounds (**4f**, **4h**, **4n**, **5f** and **5m**) were evaluated against MTB $H_{37}Rv$ grown under hypoxic and normal oxygen conditions. The low oxygen recovery assay (LORA) protocol was followed for the evaluation under hypoxic conditions [44], whereas the minimum bactericidal concentration (MBC) and MIC were determined against MTB $H_{37}Rv$ grown under aerobic conditions in 7H9-Tw-OADC medium. The outcome of these experiments revealed compound **4f** most potent under low oxygen level at an exciting IC_{50} of 0.65 μM and at normal oxygen level with IC_{50} 1.6 μM. Further, the MBC value obtained for **4f** was also notable (IC_{50} = 11.5 μM). Similarly, the thiomorpholine tethered compound **5f** also exhibited comparatively high inhibition at normal oxygen level with an impressive IC_{50} of 2.2 μM than the hypoxic condition (IC_{50} = 5.2 μM). Moreover, **5f** displayed highest inhibition (MBC = 7 μM) than **4f**, which is also evident for the promising anti-mycobacterial activity (Table 3).

2.2.4. *Cytotoxicity and intracellular anti-mycobacterial activity assays*

Cytotoxicity and intracellular anti-mycobacterial activity of the five most active compounds were assessed by employing THP-1 human monocytic cell line, and THP1 cells infected with MTB, respectively [45]. As it was obvious for the isatin-based medicinal compounds were cytotoxic [46], the tested compounds showed moderate cytotoxicity. Of the tested compounds, the intracellular activity of **4f** and **5f** was higher at IC_{50} of 6.0 μM and 6.5 μM, respectively which specified higher potency (Table 3).

Table 3
Anti-mycobacterial activity (under hypoxic and under aerobic), MBC, cytotoxicity and intracellular activity of the selected compounds (**4f**, **4n**, **4h**, **5f** and **5m**) against *M. tuberculosis* $H_{37}Rv$ grown under various conditions.

Compound	Anti-mycobacterial activity						Minimum Bactericidal Concentration[b] (MBC, μM)	Cytotoxicity [c] IC_{50} (μM)	Intracellular Activity (against *M. tuberculosis*) [d]	
	Under Low Oxygen[a]			Under aerobic						
	MIC (μM)	IC_{50} (μM)	IC_{90} (μM)	MIC (μM)	IC_{50} (μM)	IC_{90} (μM)			IC_{50} (μM)	IC_{90} (μM)
4f	> 200	**0.65**	13	4.5	**1.6**	4.4	**11.5**	0.39^	**6**	16
4*n*	130	8	30	41	20	> 50	17	2.9	18	35
4h	80	24	42	23	12	23	12	3.8	14	22
5f	50	**5.2**	33	4.4	**2.2**	4.8	**7**	0.84^	**6.5**	10
5m	39	16	24	41	17	44	28	5.2	15	19
Rifampicin	0.13[#]	0.00041[#]	0.0065[#]	0.0096[#]	0.00072[#]	0.0025[#]	ND	ND	ND	ND
Metronidazole	200[$]	29[$]	110[$]	> 200[$]	> 200[$]	> 200[$]	ND	ND	ND	ND
Staurosporine	ND	ND	ND	ND	ND	ND	ND	0.018	ND	ND
Isoniazid	ND	ND	ND	ND	ND	ND	ND	ND	0.23	0.29

[a] Organisms grown under hypoxic conditions were assessed using LORA assay.
[b] Organisms were grown under aerobic conditions in 7H9-Tw-OADC medium.
[c] Cytotoxicity was determined using the human monoocytic (THP-1) cell line.
[d] Intracellular activity was determined using THP1 infected with *M. tuberculosis*.
[#] Calculated averages for rifampicin for each run (number of replicates 6).
[$] Metronidazole was run as a control once in each run.
^ compounds found to be cytotoxic; ND: Not determined.

2.2.5. Anti-mycobacterial evaluation against other disease relevant mycobacterial species

The compounds **4f**, **4h**, **4n**, **5f** and **5m** were also screened for their *in vitro* anti-TB activity against other disease-relevant *Mycobacterial* species such as *Mycobacterium abscessus* and *Mycobacterium avium* using MABA method [47]. .

The activity data demonstrated a moderate anti-mycobacterial activity for the compound **5 m** towards *M. avium* (IC_{50} = 50 μM) than *M. abscessus* (MIC = 84 μM). However, remaining compounds did not show notable inhibition against the screened *Mycobacterial* species (Table 4).

2.2.6. Structure-activity relationship (SAR) studies

Fig. 2 presents anti-TB spectrum of activity profiles of the most active compounds **4f** and **5f**. The SAR analysis indicated the plausible reason for the highest inhibition and could be attributed to the presence of more reactive 5-membered heterocyclic thiophene moiety substituted with highly electron-withdrawing nitro (NO_2) group. In the absence of nitro substitution on five-membered thiophene/furyl ring, a decrease in the activity was observed. A systematic SAR study through the analysis of level-I and level-II results paved a way towards the discovery of the lead compounds **4f** and **5f**, wherein the latter being the most active against the multidrug-resistant strains of MTB, exclusively.

2.3. In silico study

2.3.1. Molecular docking studies

The molecular docking tool, GLIDE, was used for ligand docking studies into the *Mycobacterial* ATP synthase enzyme binding pocket. Docking methodology was validated by measuring RMSD of the co-crystalized (internal) ligand and extracted internal ligand of the docked target protein–ligand complex structure, which served as a control docking model as shown in Fig. 3. The docking result showed that Glide SP docking evaluated the optimal orientation of the co-crystallized ligand. RMSD value of 1.123 suggested that the methodology was perfect for predicting the binding affinity for unknown ligands. Docking result demonstrated that potent compounds **4f**, **4n**, **4h**, **5f**, **5m** also shown significant docking score with GyrB ATPase domain as shown in Table 5. The indolin-2-one derivative **4f** showed the hydrogen bond interaction with the Asp79 and Arg141 *via* the NH and NO_2 functional group. Similarly, *N*-substituted indolin-2-one derivative **5f** showed hydrogen bond interaction with the Arg141 and Glu48 *via* the NO_2 functional group and nitrogen of thiomorpholine ring as given in Fig. 4. .

Table 4
Anti-mycobacterial activity of the selected compounds (**4f**, **4n**, **4h**, **5f** and **5m**) against other disease-relevant *Mycobacterial* species.

Compound	*M. abscessus*[a]			*M. avium*[b]
	MIC (μM)	IC_{50} (μM)	IC_{90} (μM)	MIC (μM)
4f	> 200	> 200	> 200	> 200
4*n*	> 200	> 200	> 200	100
4h	190	> 200	> 200	> 200
5f	> 100	180	> 100	> 100
5m	98	**84**	90	**50**
Rifampicin	3.3	2.1	3.1	0.1

[a] *M. abscessus* subsp. *bollettii* 103.
[b] *M. avium* subsp. *avium* 2285 (S).

2.3.2. MM-GBSA binding free energy analysis

MM-GBSA binding free energy analysis was carried out of the nine potent protein–ligand complexes along to assess the affinity of ligands to the target proteins. The binding free energies (ΔG_{Bind}) evaluated by this method are more efficient than the Glide score values for the assortment of protein–ligand complexes. The primary energy components, such as Coulomb or Electrostatics Interaction energy ($\Delta G_{Bind\ Coulomb}$), Lipophilic Interaction energy ($\Delta G_{Bind\ Lipo}$), Generalized Born electrostatic solvation energy ($\Delta G_{Solv\text{-}GB}$) and van der Waals interaction energy ($\Delta G_{Bind\ vdW}$) altogether contribute to the analysis of MM-GBSA-based relative binding affinity. The binding energies and the contributing factors calculated for the protein dock complexes are mentioned in Table 6. Among all the studied complexes, **4i** complex showed high binding free energies (ΔG_{Bind} = -58.49 Kcal/mol). Among the *in vitro* tested potent compounds; **5f** (ΔG_{Bind} = -53.48 Kcal/mol), **4n** (ΔG_{Bind} = -51.93 Kcal/mol), **4f** (ΔG_{Bind} = -51.93 Kcal/mol), and **4h** (ΔG_{Bind} = -50.63 Kcal/mol) have shown significant binding free energy (Table 6). Correlation between docking score and binding free energy is given in Fig. 5.

2.3.3. ADME prediction and drug likeliness

In order to describe the drug-likeliness of the hybrids **4(a-o)** and **5(a-o)**, we screened them for Lipinski's rule of five, wherein the molecular properties will be correlated with the oral bioavailability of the respective molecules. QikProp of Schrodinger Maestro-12.1 [48] was employed for the computation of various parameters and the results are

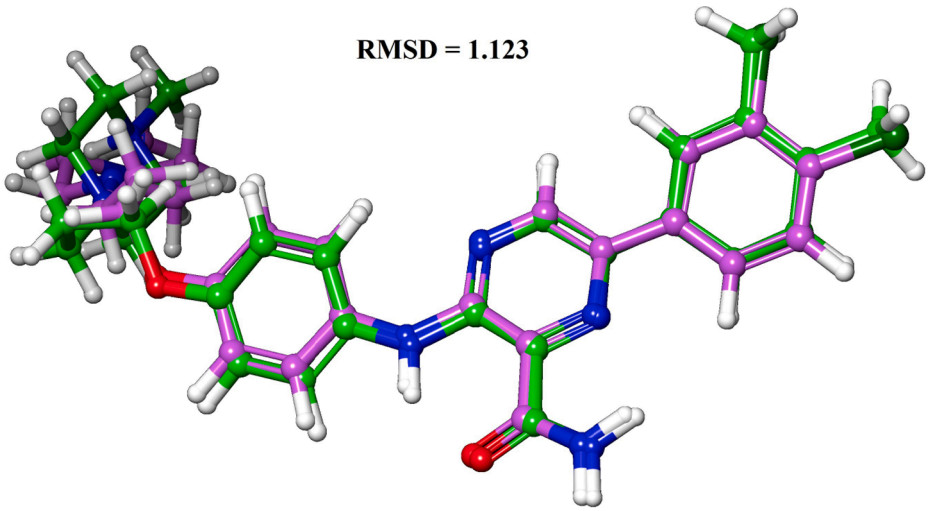

Fig. 3. The impeccably overlapped conformation of the docked ligand B5U (purple-coloured carbon backbone) with respect to its crystallized conformation (green-coloured carbon backbone) obtained from the bioactive complex structure 4B6C. (For interpretation of the references to colour in this figure legend, the reader is referred to the web version of this article.)

Table 5
Glide SP docking score of the synthesized compounds.

Compound Code	Docking Score	Glide Rewards	Glide Emodel	Glide Energy
4k	−7.785753	−2.357329	−58.680619	−42.229731
4f	−7.723262	−2.482856	−59.216648	−43.842531
4*n*	−7.723262	−2.482856	−59.216648	−43.842531
4l	−7.613359	−2.435352	−58.15461	−41.869961
5f	−7.604208	−2.016184	−69.982567	−51.69332
4h	−7.532954	−2.553628	−58.3836	−42.20331
4g	−7.506493	−2.586952	−54.185238	−38.379974
4i	−7.428364	−2.154589	−61.148719	−44.141524
4d	−7.424273	−2.668566	−55.929295	−40.288377
5b	−7.397044	−1.70923	−67.573204	−51.766265
4o	−7.354074	−2.335253	−57.837476	−42.504819
4j	−7.340918	−1.73906	−63.44352	−45.544755
5a	−7.333291	−1.973769	−67.868708	−48.858482
5m	−7.288588	−2.146985	−64.171054	−46.504151
4b	−7.262156	−1.982486	−62.303222	−43.975905
4a	−7.189469	−2.392884	−58.709521	−41.692272
4m	−7.176897	−2.665586	−54.333397	−36.874597
5d	−7.10449	−2.118613	−61.625476	−45.64237
4e	−7.035323	−2.801185	−51.197577	−37.296104
5h	−7.003703	−2.073834	−68.163663	−53.305054
5e	−6.965062	−2.264101	−60.682799	−44.348117
5g	−6.927207	−2.117143	−61.909195	−45.570659
5i	−6.884912	−1.673494	−64.268893	−47.53827
5j	−6.705468	−1.467624	−65.6246	−48.558695
5*n*	−6.696261	−1.663096	−68.78346	−53.610616
4c	−6.691652	−2.604747	−53.698382	−39.778039
5o	−6.596076	−2.03999	−63.272763	−47.863721
5c	−6.536609	−2.038783	−64.697257	−47.713697
5 k	−6.494694	−1.863428	−61.291287	−47.696196
5 l	−6.169308	−1.460659	−65.784868	−49.724288

summarized in Table 7. Remarkably, all the synthesized hybrid compounds were found to be in agreement with Lipinski's rule of five [49] and Jorgensen's rule of three as well. The pharmacokinetic ADME properties play significant roles in the determination of the safety and efficacy of drug-like compounds. Human intestinal absorption (HIA) and Caco-2 permeability (QPPCaco) parameters are the best markers of the absorption of the drug in the intestine and Caco-2 monolayer penetration, respectively. HIA data are the sum of bioavailability and absorption evaluated from the ratio of excretion or cumulative excretion in urine, bile, and feces [50]. Moreover, QPPCaco permeability parameter acts as a crucial feature regulating the metabolism of drugs [51]. The predicted percentages of human oral absorption for the hybrids were found to be>80% and QPPCaco values were > 500 with the exception of **4f**, **4h**, **4n**, **5f**, **5 h**, and **5n**. The partition coefficient (QPlogPo/w) and water solubility (QPlogS) are also important parameters for the absorption and distribution of the drugs [52]. QPlogPo/w and QPlogS values were computed, which ranged from 1.033 to 3.401 and −4.365 to −0.303, respectively. Thus, QikProp predicted the physico-chemically crucial descriptors and pharmaceutically relevant properties, all of which established that the hybrids confer good drug-like properties (Table 7 and footnote) and can be considered for the further drug development events.

2.3.4. *Molecular dynamic simulation study*

A molecular docking study was performed using the rigid crystal structure of GyrB ATPase domain. Hence, we have evaluated target and lead compounds interactions in the dynamic behavior using molecular dynamic simulation to obtain the stable binding conformation. Compound **5f** in complex with GyrB ATPase domain was considered for the molecular dynamic simulation for 10 ns, using simple point charge (SPC) water mode. The Root Mean Square Deviation (RMSD), Root Mean Square Fluctuation (RMSF), and Protein-Ligand Contacts were analyzed from the MD simulation trajectories to study thermodynamic conformational stability during 10 ns period. MD simulation trajectories' RMSD analysis denotes the protein backbone's stability, when bound with the specific ligand within the dynamic condition. It also provides brief insights into its structural conformation during the MD simulation. Lower RMSD value throughout the MD simulation suggests the higher stability of the protein–ligand complex, whereas higher RMSD value shows comparatively low stability of the protein–ligand complex [34,39].

The RMSD graph result of compound **5f** is shown in Fig. 6. Initially, ligand was unstable at around 3 ns with RMSD of the graph line showed an increasing trend from 0 to 10 ns with RMSD value of 4.4 Å. After 4 ns, the promising result was observed, and the graph line was stable till 10 ns. The overall RMSD analysis revealed that fluctuations in a graph during 10 ns simulation are within the standard range of RMSD. Ligand RMSD of 1–3.6 Å indicates that the compound **5f** bound tightly within the cavity of GyrB ATPase domain. The RMSF value represents the mobility and flexibility of each protein residue during the entire simulation. Greater the RMSF values indicate more flexibility during the MD simulation, while the lower value of RMSF reflects the stability of the system [34]. Compound **5f**-GyrB ATPase domain complex yielded little fluctuations up to 2 Å, which is perfectly acceptable Fig. 7.

Protein-ligand interactions can be monitored throughout the

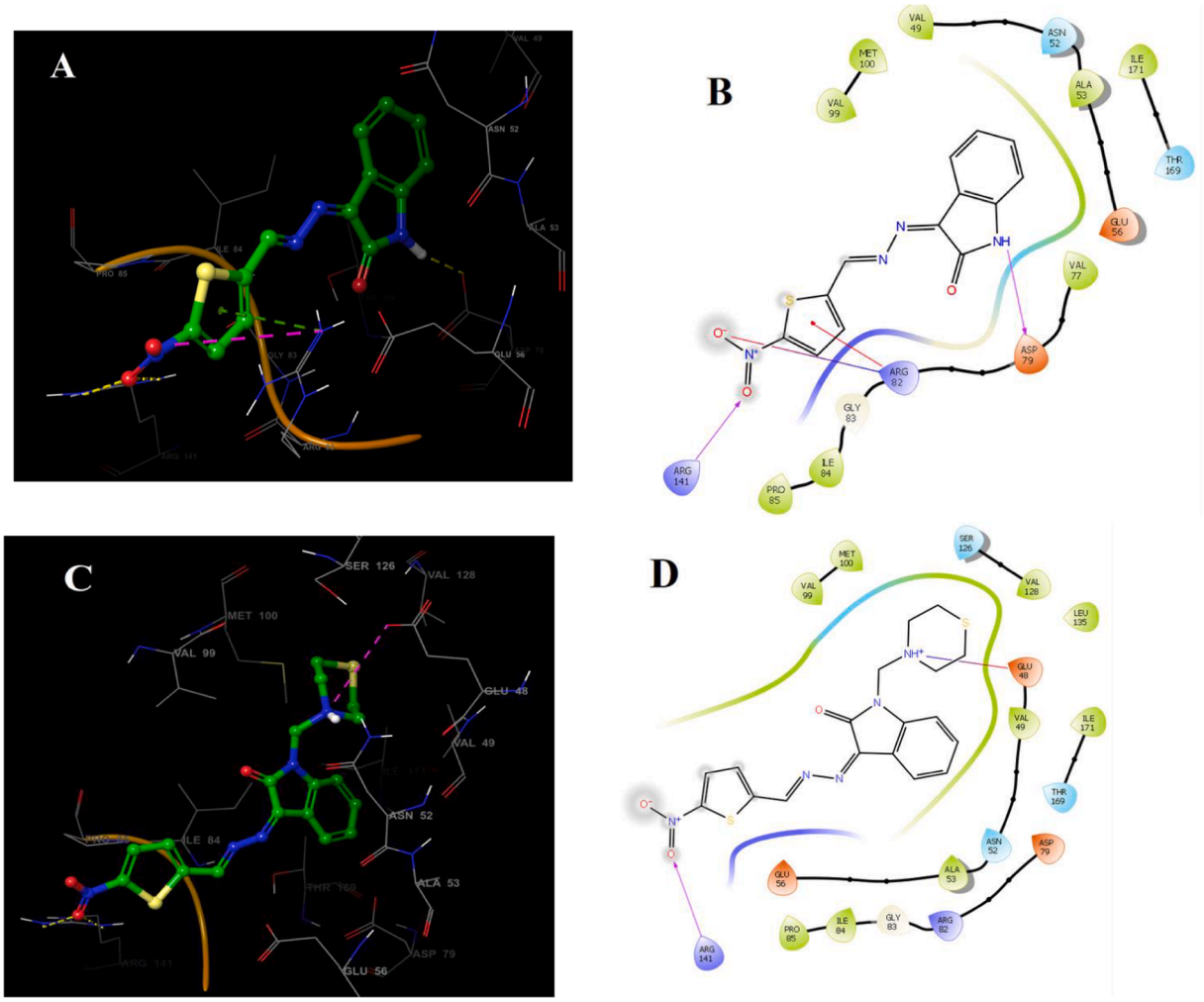

Fig. 4. Binding interaction of the compounds **4f** (A: 3D view; B: 2D view) and **5f** (C: 3D view; D: 2D view) with GyrB ATPase domain.

simulation (Fig. 8). Nitrogen of thiomorpholine ring of compound **5f** is forming direct hydrogen bond with Asn52 and water mediated hydrogen bond with Val99 and Val125. Residue Glu65 played a crucial role in forming a hydrogen bond with nitro functional group and water mediated hydrogen bond with hydrazone nitrogen of compound **5f**. Arg82 formed π-π stacking with thiophene ring of the compound **5f**.

Additionally, the Fig. 9 shows the total number of specific contacts protein makes with ligand throughout the trajectory. The contribution of amino acids in each trajectory frame of 10 ns MD simulation as shown in the bottom panel of Fig. 9, which represent the number of contacts and their density (the darker shade of orange shows more than one contact in that frame). Key interaction seen during each frame was with hydrophobic residue Ile84 and Pro85, which was consistent during the complete simulation process. Other interactions were also found with Val99, Val125, Ile171 and His89, which were not consistent during the simulation.

3. Conclusion

In summary, isatin hydrazones **4(a-o)** and their thiomorpholine analogs **5(a-o)** were synthesized, characterized and screened at level-I against MTB $H_{37}Rv$ for their anti-mycobacterial activity. From the two series, five most active compounds **4f**, **4h**, **4n**, **5f** and **5m** were selected for level-II screening. Compounds **4f** and **5f** emerged as the most potent compounds exhibiting highest inhibition against both the normal ($H_{37}Rv$) and drug-resistant MTB strains, which could be attributed to the presence of 5-nitrothiophene hydrazone moiety in their structures. The results indicated that both **4f** and **5f** were mostly equipotent against the drug-resistant MTB strains, however closer analysis of the data revealed that **4f** was specifically more active against INH-R1 and R2 (IC_{50} = 3.5 and 4.6 μM), while compound **5f** was explicitly found best active against rifampicin-resistant (RIF-R1) strain with a potent IC_{50} value 1.9 μM, followed by isoniazid-resistant INH-R1 (IC_{50} = 3.4 μM) and INH-R2 (IC_{50} = 5.3 μM) strains, respectively. Moreover, **4f** and **5f** established interesting IC_{50} at 5.9 μM and 4.9 μM, respectively against fluoroquinolone-resistant (FQ-R1) MTB strain that indicated the possibility of further exploiting these compounds for developing potential XDR anti-TB agents. These exciting activity profiles of the lead compounds **4f** and **5f** suggested that they can be further optimized to develop highly potent anti-mycobacterial drugs for the treatment of both MDR-TB and XDR-TB infections. Molecular docking results revealed crucial ligand-protein interactions, while MD simulation suggested that the complex was stable for 10 ns in the GyrB ATPase domain. *In silico* computation of pharmacokinetic properties of all the synthesized compounds were found to be in agreement within the acceptable ranges. Based on the identified lead structures **4f** and **5f**, further synthesis and anti-mycobacterial screening against multidrug-resistant TB strains are currently in progress to obtain novel drug candidates exhibiting potency at nanomolar ranges, while retaining the safety profiles.

4. Experimental

All the chemicals used in this research work were purchased from

Table 6
Binding free energy components for the protein ligand complexes calculated by MM-GBSA analysis.

Compound Code Code	MMGBSA (Kcal/mol)					Prime Energy
	ΔG Bind	ΔG Coulomb	ΔG Lipo	ΔG Solv_GB	ΔG vdW	
4k	−53.81	−11.33	−17.58	22.26	−44.51	−14335.05
4f	−51.93	−1.41	−17.25	15.37	−46.02	−14333.05
4*n*	−51.93	−1.41	−17.25	15.37	−46.02	−14333.05
4l	−44.73	−3.36	−20.72	21.25	−46.89	−14335.9
5f	−53.48	−7.42	−22.26	15.47	−57.62	−14309.4
4h	−50.63	−5.37	−16.07	16.45	−43.1	−14326.58
4g	−48.14	−10.64	−16.98	23.79	−41.75	−14320.36
4i	−58.49	−13.49	−20.31	26.76	−48.9	−14348.02
4d	−39.62	−1.23	−19.35	19.76	−44.01	−14324.85
5b	−50.31	−1.88	−23.49	29.32	−59.51	−14286.36
4o	−54.47	−11.58	−18.6	23.04	−44.61	−14332.3
4j	−52.76	−1.8	−20.15	20.89	−53.24	−14322
5a	−53.12	−1.07	−21.18	27.31	−57.14	−14309.15
5m	−48.16	−0.37	−20.21	24.99	−54.26	−14298.68
4b	−51.82	−0.86	−19.29	21.43	−51.2	−14315.2
4a	−51.44	−12.35	−18.73	28.12	−45.87	−14335.05
4*m*	−46.7	−1.09	−19.68	16.01	−42.29	−14331.81
5d	−49.58	−1.67	−18.67	24.37	−52.05	−14302.68
4e	−37.73	−3.11	−17.47	21.45	−39.38	−14314.99
5 h	−57.77	−9.44	−20.01	22.87	−54.07	−14306.45
5e	−44.5	−0.04	−17.89	23.29	−52.29	−14296.43
5g	−47.39	−0.1	−19.89	24.61	−54.42	−14294.48
5i	−50.53	−0.92	−23.01	28.09	−60.21	−14315.31
5j	−51.04	−1.99	−23.79	29.41	−62.72	−14295.47
5*n*	−52.38	−2.8	−20.72	23.56	−58.36	−14314.87
4c	−45.1	−6.17	−15.5	20.51	−39.02	−14320.96
5o	−51.05	−8.2	−21.25	27.62	−54.67	−14304.51
5c	−46.6	−7.75	−19.54	30.32	−55.34	−14302.88
5 k	−52.66	−9.91	−20.43	27.42	−54.35	−14309.22
5 l	−53.57	−16.43	−22.19	31.63	−44.28	−14313.41

ΔG Bind: Binding free Energy; **ΔG Coulomb**: Coulomb or Electrostatics Interaction energy; **ΔG Lipo**: Lipophilic Interaction energy; **ΔG Solv_GB**: Generalized Born electrostatic solvation energy, **ΔG vdW** : Van der Waals Interaction energy.

Sigma-Aldrich and Merck Millipore, South Africa. All the solvents, except those of reagent grade, were dried and purified when necessary, according to previously published methods. The progress of the reactions and the purity of the compounds were monitored by thin-layer chromatography (TLC) on pre-coated silica gel plates procured from E. Merck and Co. (Darmstadt, Germany). The melting points of the synthesized compounds were determined using a Thermo Fisher Scientific (IA9000, UK) digital melting point apparatus and are uncorrected. The IR spectra were recorded on a Bruker Alpha FT-IR spectrometer (Billerica, MA, USA) using the ATR technique. The ^{1}H NMR and ^{13}C NMR spectra were recorded on a Bruker AVANCE 400 and 100 MHz (Bruker, Rheinstetten/Karlsruhe, Germany) spectrometer, respectively using the solvent DMSO-d_6. The chemical shifts (δ) reported are given in parts per million (ppm) and the coupling constants (J) are in Hertz (Hz) values with respect to TMS as an internal standard. The spin multiplicities are reported as s = singlet, d = doublet, t = triplet, dd = doublet of doublet and m = multiplet. HRMS spectra were recorded on an Autospec mass spectrometer with electron impact at 70 eV.

4.1. Synthesis of compounds 2a and 2b

Compounds **2a** and **2b** were synthesized in good yields according to the reported procedure [37,38].

4.2. General procedure for the synthesis of (Z)-3-(((E)-arylidene) hydrazono)indolin-2-one 4(a-o)

The stirred solution of hydrazonoindolones **2a** or **2b** (2 mmol) in ethanol (5 ml) was placed in a microwave reactor vial (10 ml capacity), corresponding aldehydes **3** (2.4 mmol), and 3 drops of acetic acid were added subsequently irradiated at 80 °C for 10 min in the CEM microwave reactor. Upon completion of the reaction, the mixture was filtered, washed with ethanol and dried to obtain the desired 3-arylidenehydrazono indolin-2-ones **4(a-o)** in good yields.

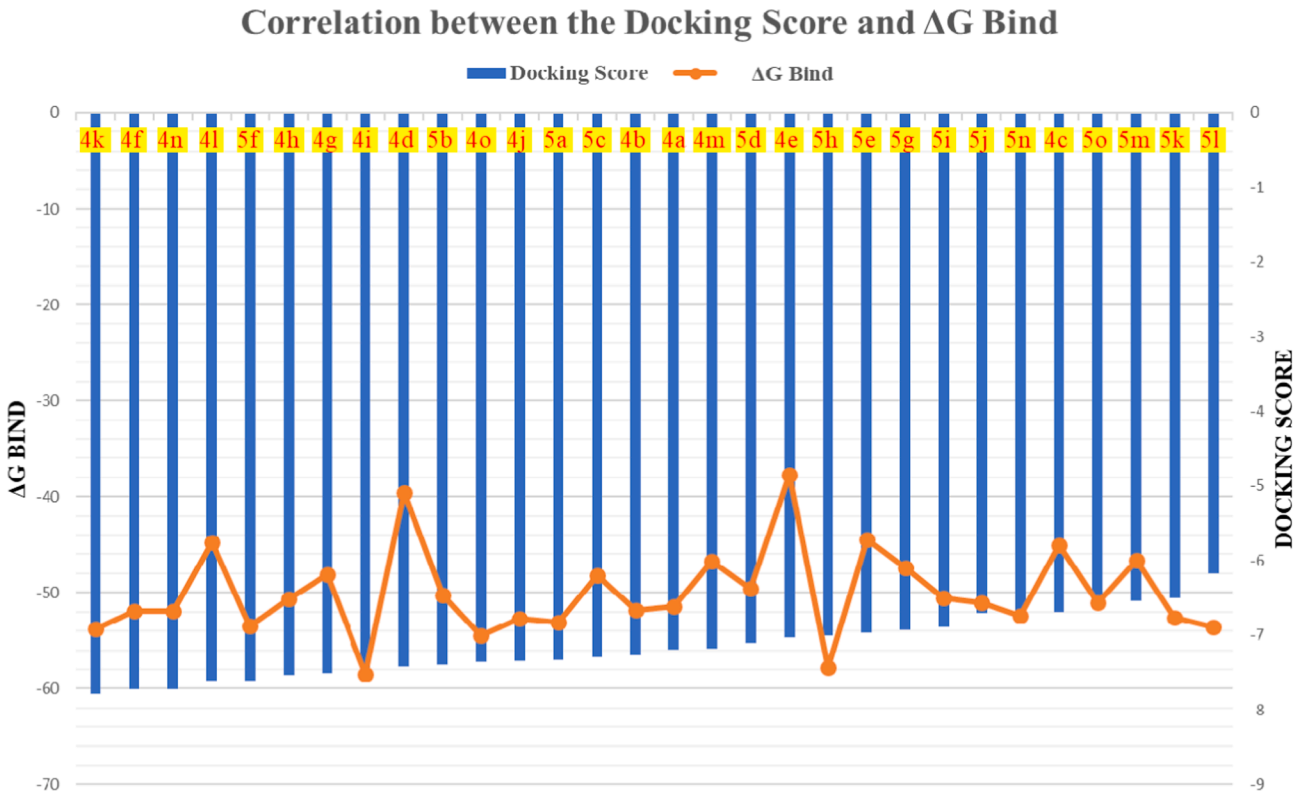

Fig. 5. The correlation plot between MM-GBSA (**ΔG Bind**) values (primary y-axis) and docking score (secondary y-axis) of the synthesized compounds.

Table 7
The drug likeliness and *in silico* ADME properties of **4(a-o)** and **5(a-o)** calculated using QikProp.

Entry	Drug likeliness (Lipinski's rule of five)					*In silico* ADME by QikProp						
	Molecular weight	QPlogP O/W[a]	H-bond donor	H-bond acceptor	Violation of Lipinski's rule	QPlogS[b]	QPlogHERG[c]	QPPCaco[d]	QPPMDCK[e]	QPlogKhsa[f]	% human oral absorption[g]	Violation of rule of three
4a	279.298	2.231	1	5.75	0	−3.194	−5.366	1287.917	650.318	−0.206	95.66	0
4b	309.324	2.317	1	6.50	0	−3.499	−5.339	1098.810	547.750	−0.196	94.93	0
4c	250.259	1.227	1	6.50	0	−2.492	−5.350	599.360	284.483	−0.497	83.84	0
4d	255.294	2.128	1	5.00	0	−3.126	−5.306	1225.380	1133.156	−0.263	94.67	0
4e	239.233	1.489	1	5.50	0	−2.288	−5.039	1164.595	583.280	−0.448	90.54	0
4f	300.291	1.415	1	6.00	0	−3.099	−5.263	173.470	102.239	−0.309	75.30	0
4g	250.259	1.238	1	6.50	0	−2.491	−5.345	613.566	291.779	−0.495	84.09	0
4h	284.231	1.033	1	6.50	0	−2.598	−5.263	199.110	86.448	−0.461	74.14	0
4i	313.743	2.705	1	5.75	0	−3.828	−5.308	1262.277	1567.580	−0.102	100	0
4j	343.769	2.813	1	6.5	0	−3.797	−4.902	1695.044	2164.534	−0.143	100	0
4k	284.704	1.816	1	6.50	0	−3.336	−5.481	675.204	798.639	−0.375	88.22	0
4l	289.739	2.588	1	5.00	0	−3.800	−5.201	1217.922	2775.490	−0.163	100	0
4m	273.678	1.919	1	5.50	0	−2.897	−4.868	1138.978	1403.968	−0.358	92.89	0
4*n*	334.736	1.840	1	6.00	0	−3.920	−5.411	143.574	189.250	−0.200	76.32	0
4o	284.704	1.777	1	6.50	0	−3.144	−5.236	719.589	854.116	−0.390	88.48	0
5a	394.490	2.525	0	8.75	0	−1.858	−6.160	948.479	942.709	−0.508	95.01	0
5b	424.517	2.451	0	9.50	0	−1.608	−6.020	837.312	803.023	−0.592	93.60	0
5c	365.452	1.301	0	9.50	0	−0.303	−5.651	630.381	567.796	−0.997	84.67	0
5d	370.486	2.461	0	8.00	0	−3.122	−6.092	790.597	1456.302	−0.509	93.22	0
5e	354.426	1.892	0	8.50	0	−1.313	−6.201	784.503	770.261	−0.722	89.93	0
5f	415.484	1.652	0	9.00	0	−1.534	−5.981	142.208	139.415	−0.649	75.13	0
5g	365.452	1.386	0	9.50	0	−0.761	−5.817	441.444	415.365	−0.906	82.40	0
5h	399.423	1.276	0	9.50	0	−1.254	−6.213	143.231	123.566	−0.833	73.00	0
5i	428.935	2.998	0	8.75	0	−2.833	−6.290	790.810	1933.578	−0.370	96.37	0
5j	458.962	3.401	0	9.50	0	−4.365	−6.515	761.076	1851.636	−0.260	100	0
5k	399.897	2.033	0	9.50	0	−1.839	−6.217	602.086	1428.073	−0.769	88.60	0
5l	404.931	2.977	0	8.00	0	−2.706	−5.964	934.259	4277.038	−0.399	100	0
5m	388.871	2.378	0	8.50	0	−2.065	−6.099	769.902	1878.658	−0.597	92.53	0
5*n*	449.929	2.135	0	9.00	0	−2.321	−5.995	154.992	389.882	−0.547	78.64	0
5o	399.897	1.758	0	9.50	0	−1.506	−5.821	399.574	920.604	−0.819	83.80	0

[a] Predicted octanol/water partition co-efficient log p (acceptable range from −2.0 to 6.5).
[b] Predicted aqueous solubility in mol/L (acceptable range: −6.5 to 0.5).
[c] Predicted IC_{50} value for blockage of HERG K + channels (concern below −5.0).
[d] Predicted Caco-2 cell permeability in nm/s (acceptable range: <25 is poor and >500 is good).
[e] Predicted apparent MDCK cell permeability in nm/s (acceptable range: <25 is poor and > 500 is good).
[f] Prediction of binding to human serum albumin (acceptable range: −1.5 to 1.5).
[g] Percentage of human oral absorption (<25% is poor and > 80% is high).

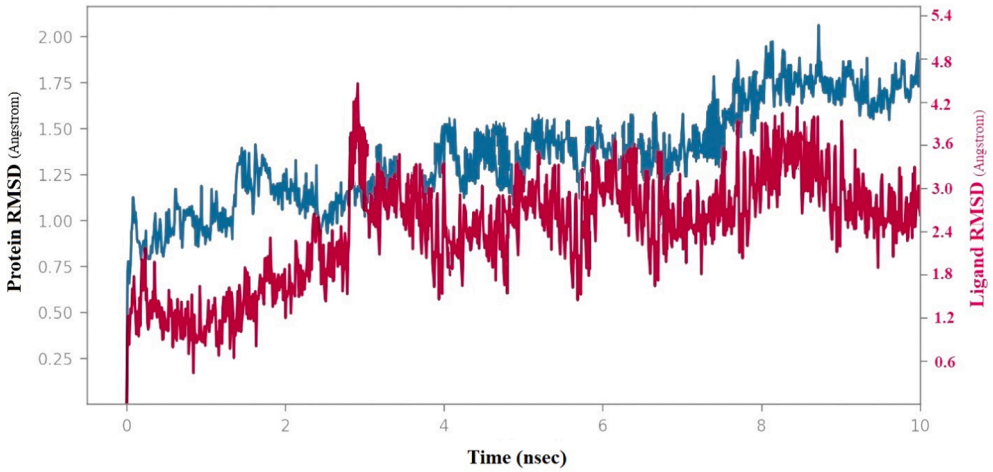

Fig. 6. Time-dependent Protein-ligand RMSD plot (Angstrom) of the compound **5f** with GyrB ATPase domain.

4.2.1. (Z)-3-(((E)-4-methoxybenzylidene)hydrazono)indolin-2-one (4a)

Crimson red solid; Yield: 82%; mp: 192–194 °C; FTIR (ATR, ν_{max}, cm^{-1}): 1457 (Aromatic C═C stretch), 1510 (N—H bend), 1597 (C═O), 1714 (C═N), 3133 (N—H stretch); ^{1}H NMR (400 MHz, DMSO-d_6): δ = 3.85 (s, 3H, –OCH_3), 6.89–8.90 (t, J = 7.76 Hz, 1H, ArH), 7.02–7.06 (t, J = 7.54 Hz, 1H, ArH), 7.12–7.14 (d, J = 8.80 Hz, 2H, ArH), 7.37–7.41 (dt, J = 7.71 Hz, 1H, ArH), 7.94–7.97 (d, J = 8.76 Hz, 2H, ArH), 8.03–8.05 (d, J = 7.52 Hz, 1H, ArH), 8.63 (s, 1H, N═C-H), 10.82 (s, 1H, –NH) ppm; ^{13}C NMR (100 MHz, DMSO-d_6): δ = 55.51, 110.71, 114.74, 116.61, 122.27, 126.03, 128.84, 130.99, 133.33, 144.81, 150.63, 161.93, 162.60, 164.71 ppm.

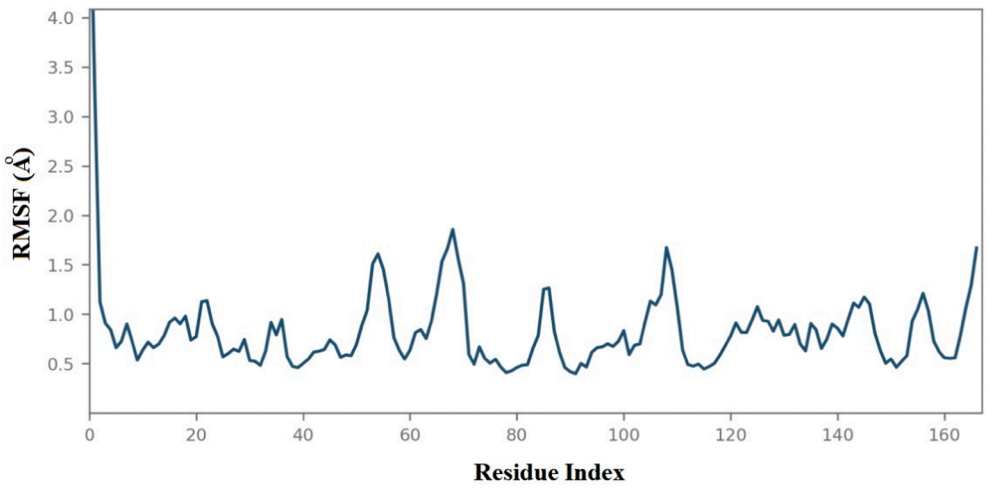

Fig. 7. Time-dependent Protein RMSF plot (Angstrom) of the compound **5f** with GyrB ATPase domain.

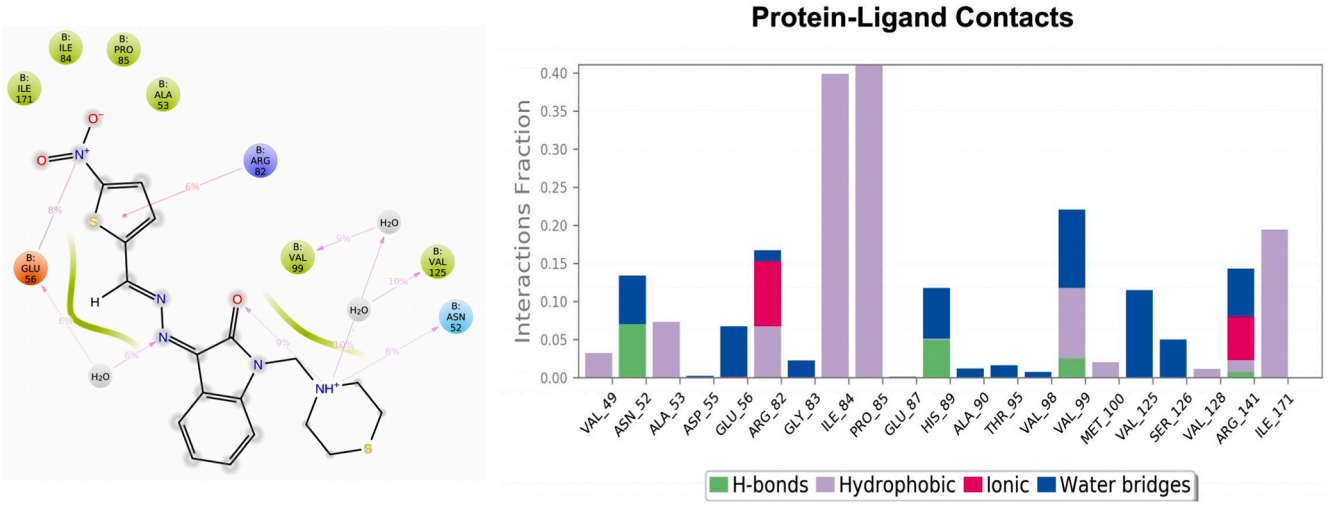

Fig. 8. Simulation Interactions Diagram, 2D binding interaction of the compound **5f** with GyrB ATPase domain along with bar diagram.

4.2.2. (Z)-3-(((E)-3,4-dimethoxybenzylidene)hydrazono)indolin-2-one (4b)

Crimson red solid; Yield: 79%; mp: 221–223 °C; FTIR (ATR, ν_{max}, cm^{-1}): 1449 (Aromatic C═C stretch), 1500 (N—H bend), 1606 (C═O), 1709 (C═N), 3133 (N—H stretch); ^{1}H NMR (400 MHz, DMSO-d_6): δ = 3.85 (s, 3H, –OCH_3), 3.86 (s, 3H, –OCH_3), 6.88–6.90 (d, J = 7.84 Hz, 1H, ArH), 7.01–7.05 (t, J = 7.72 Hz, 1H, ArH), 7.11–7.13 (d, J = 8.20 Hz, ArH), 7.35–7.39 (dt, J = 7.62, 0.90 Hz, 1H, ArH), 7.52–7.55 (m, 2H, ArH), 7.99–8.01 (d, J = 7.52 Hz, 1H, ArH), 8.56 (s, 1H, N═C-H), 10.82 (s, 1H, NH) ppm; ^{13}C NMR (100 MHz, DMSO-d_6): δ = 55.47, 55.69, 110.30, 110.71, 11.72, 116.58, 122.27, 123.941, 126.12, 128.76, 133.36, 144.78, 149.09, 150.48, 152.46, 161.41, 164.71 ppm.

4.2.3. (Z)-3-(((E)-pyridin-3-ylmethylene)hydrazono)indolin-2-one (4c)

Brick red solid; Yield: 78%; mp: 201–203 °C; FTIR (ATR, ν_{max}, cm^{-1}): 1459 (Aromatic C═C stretch), 1552 (N—H bend), 1613 (C═O), 1726 (C═N), 3156 (N—H stretch); ^{1}H NMR (400 MHz, DMSO-d_6): δ = 6.88–6.90 (d, J = 7.80 Hz, 1H, ArH), 6.99–7.03 (t, J = 7.56 Hz), 7.37–7.41 (t, J = 7.64 Hz, 1H, ArH), 7.57–7.60 (m, 1H, ArH), 7.84–7.86 (d, J = 7.52 Hz, 1H, ArH), 8.35–8.37 (d, J = 7.84 Hz, 1H, ArH), 8.65 (s, 1H, N═C-H), 9.08 (s, 1H, ArH), 10.82 (s, 1H, NH) ppm; ^{13}C NMR (100 MHz, DMSO-d_6): δ = 110.85, 116.21, 122.41, 124.28, 128.90, 129.33, 133.88, 135.17, 145.13, 150.18, 152.33, 157.47, 164.32 ppm.

4.2.4. (Z)-3-(((E)-thiophen-2-ylmethylene)hydrazono)indolin-2-one (4d)

Crimson red solid; Yield: 72%; mp: 202–204 °C; FTIR (ATR, ν_{max}, cm^{-1}): 1454 (Aromatic C═C stretch), 1539 (N—H bend), 1605 (C═O), 1735 (C═N), 3088 (N—H stretch); ^{1}H NMR (400 MHz, DMSO-d_6): δ = 6.88–6.90 (d, J = 7.80 Hz, 1H, ArH), 7.01–7.05 (t, J = 7.52 Hz, 1H, ArH), 7.26–7.28 (m, 1H, ArH), 7.36–7.40 (m, 1H, ArH), 7.77–7.78 (d, J = 3.24 Hz, 1H, ArH), 7.93–7.95 (d, J = 5.00 Hz, 1H, ArH), 8.00–8.02 (d, J = 7.60 Hz, 1H, ArH), 8.91 (s, 1H, N═C-H), 10.81 (s, 1H, NH) ppm; ^{13}C NMR (100 MHz, DMSO-d_6): δ = 110.81, 116.63, 122.24, 128.81, 128.92, 133.63, 135.28, 138.42, 144.99, 151.34, 157.07, 164.66 ppm.

4.2.5. (Z)-3-(((E)-furan-2-ylmethylene)hydrazono)indolin-2-one (4e)

Yellow solid; Yield: 75%; mp: 209–211 °C; FTIR (ATR, ν_{max}, cm^{-1}): 1462 (Aromatic C═C stretch), 1543 (N—H bend), 1619 (C═O), 1731 (C═N), 3136 (N—H stretch); ^{1}H NMR (400 MHz, DMSO-d_6): δ = 6.78–6.80 (dd, J = 3.44 Hz, 1.76 Hz, 1H, ArH), 6.88–6.90 (d, J = 7.88 Hz, 1H, ArH), 7.02–7.05 (t, J = 7.54 Hz, 1H, ArH), 7.33–7.34 (d, J = 3.48 Hz, 1H, ArH), 8.07–8.09 (d, J = 9.96 Hz, 1H, ArH), 8.55 (s, 1H, N═C-H), 10.83 (s,1H, NH) ppm; ^{13}C NMR (100 MHz, DMSO-d_6): δ = 110.73, 113.14, 116.67, 119.73, 122.25, 129.01, 133.65, 144.87, 148.04, 149.03, 150.82, 151.32, 164.62 ppm.

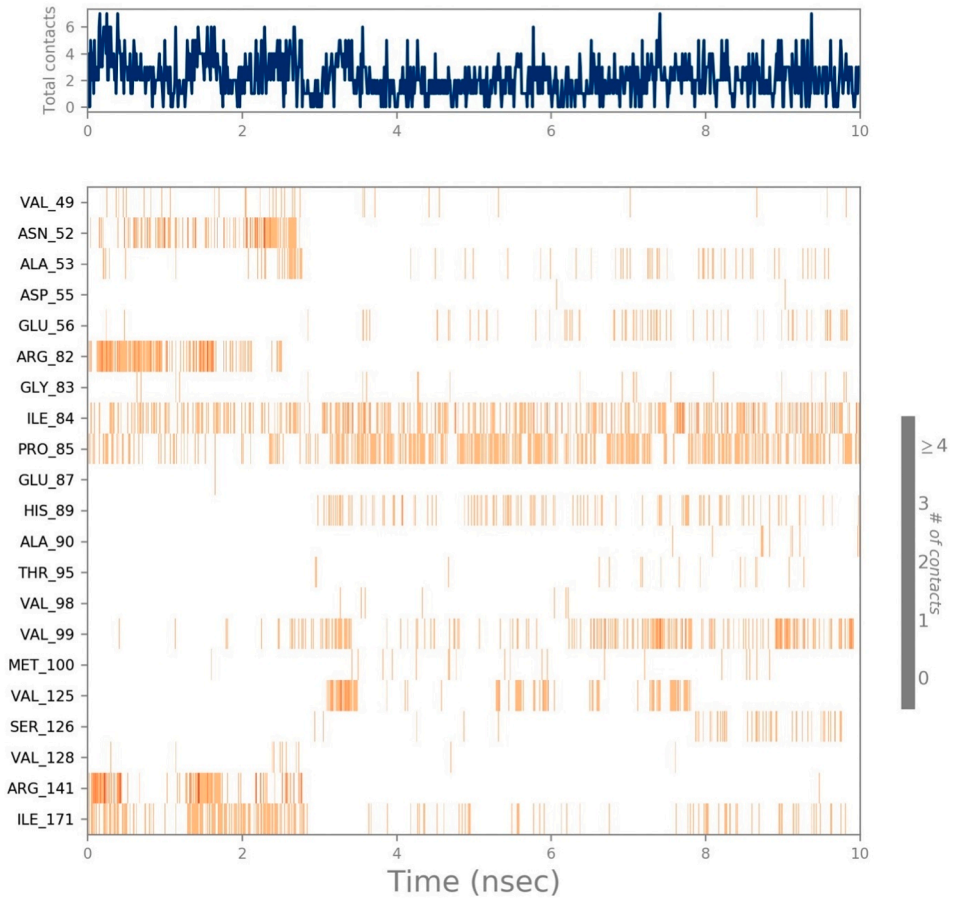

Fig. 9. Protein-Ligand contacts showing good contacts (darker shades) with the amino acid residues over 10 ns time period of simulation of the compound **5f** with GyrB ATPase domain.

4.2.6. (Z)-3-(((E)-(5-nitrothiophen-2-yl)methylene)hydrazono)indolin-2-one (4f)

Brown solid; Yield: 71%; mp: 241–243 °C; FTIR (ATR, ν_{max}, cm^{-1}): 1434 (Aromatic C═C stretch), 1526 (N—H bend), 1613 (C═O), 1725 (C═N), 3144 (N—H stretch); ^{1}H NMR (400 MHz, DMSO-d_6): δ = 6.89–6.381 (d, J = 7.84 Hz, 1H, ArH), 7.05–7.09 (t, J = 7.44 Hz, 1H, ArH), 7.40–7.44 (m, 1H, ArH), 7.7–7.79 (m, 1H, ArH), 8.20–8.21 (d, J = 4.36 Hz, 1H, ArH), 8.87 (s, 1H, N═C-H), 10.90 (s,1H, NH) ppm; ^{13}C NMR (100 MHz, DMSO-d_6): δ = 110.98, 115.98, 121.98, 122.45, 128.64, 134.09, 140.11, 145.25, 149.29, 150.67, 155.72, 164.04 ppm.

4.2.7. (Z)-3-(((E)-pyridin-4-ylmethylene)hydrazono)indolin-2-one (4g)

Yellow solid; Yield: 76%; mp: 245–247 °C; FTIR (ATR, ν_{max}, cm^{-1}): 1427 (Aromatic C═C stretch), 1556 (N—H bend), 1614 (C═O), 1725 (C═N), 3091 (N—H stretch); ^{1}H NMR (400 MHz, DMSO-d_6): δ = 6.80–6.90 (d, J = 7.76 Hz, 1H, ArH), 6.97–7.01 (t, J = 7.76 Hz, 1H, ArH), 7.37–7.41 (dt, J = 7.4 Hz, 0.8 Hz, 1H, ArH), 7.67–7.69 (d, J = 7.52 Hz, 1H, ArH), 7.84–7.86 (dd, J = 5.96 Hz, 2H, ArH), 8.51 (s, 1H, N═C-H), 8.76–8.78 (dd, J = 5.88 Hz, 2H, ArH), 10.91 (s,1H, NH) ppm; ^{13}C NMR (100 MHz, DMSO-d_6): δ = 111.07, 116.12, 122.58, 128.96, 130.52, 133.24, 134.41, 144.29, 145.52, 151.38, 154.43, 164.18 ppm.

4.2.8. (Z)-3-(((E)-(5-nitrofuran-2-yl)methylene)hydrazono)indolin-2-one (4 h)

Red solid; Yield: 73%; mp: 236–238 °C; FTIR (ATR, ν_{max}, cm^{-1}): 1460 (Aromatic C═C stretch), 1550 (N—H bend), 1614 (C═O), 1740 (C═N), 3149 (N—H stretch); ^{1}H NMR (400 MHz, DMSO-d_6): δ = 6.89–6.91 (d, J = 7.84 Hz, 1H, ArH), 7.00–7.04 (t, J = 7.52 Hz, 1H, ArH), 7.40–7.44 (dt, J = 7.75, 0.9 Hz, 1H, ArH), 7.54–7.55 (d, J = 3.96 Hz, 1H, ArH), 7.83–7.86 (m, 2H, ArH), 8.56 (s, 1H, N═C-H), 10.91 (s, 1H, NH) ppm; ^{13}C NMR (100 MHz, DMSO-d_6): δ = 110.99, 114.15, 116.11, 119.07, 122.45, 129.06, 134.3.65, 145.37, 147.25, 150.24, 150.48, 152.85, 164.11 ppm.

4.2.9. (Z)-5-chloro-3-(((E)-4-methoxybenzylidene)hydrazono)indolin-2-one (4i)

Crimson red solid; Yield: 80%; mp: 265–267 °C; FTIR (ATR, ν_{max}, cm^{-1}): 1456 (Aromatic C═C stretch), 1511 (N—H bend), 1606 (C═O), 1736 (C═N), 3143 (N—H stretch); ^{1}H NMR (400 MHz, DMSO-d_6): δ = 3.86 (s, 3H, –OCH_3), 6.91–6.93 (d, J = 8.40 Hz, 1H, ArH), 7.15–7.17 (d, J = 8.76 Hz, 2H, ArH), 7.44–7.46 (dd, J = 8.36 Hz, 2.20 Hz, 1H, ArH), 7.92–7.94 (d, J = 8.76 Hz, 2H, ArH), 8.00–8.01 (d, J = 2.02 Hz, 1H, ArH), 8.68, (s, 1H, N═C-H), 10.96 (s, 1H, NH) ppm; ^{13}C NMR (100 MHz, DMSO-d_6): δ = 55.57, 112.32, 114.91, 117.73, 125.75, 125.80, 128.01, 131.10, 143.55, 150.00, 162.90, 163.41, 164.41 ppm.

4.2.10. (Z)-5-chloro-3-(((E)-3,4-dimethoxybenzylidene)hydrazono) indolin-2-one (4j)

Crimson red solid; Yield: 78%; mp: 285–287 °C; FTIR (ATR, ν_{max}, cm^{-1}): 1456 (Aromatic C═C stretch), 1507 (N—H bend), 1616 (C═O), 1739 (C═N), 3153 (N—H stretch); ^{1}H NMR (400 MHz, DMSO-d_6): δ = 3.87 (s, 3H, –OCH_3), 3.88 (s, 3H, –OCH_3), 6.90–6.92 (d, J = 8.36 Hz, 1H, ArH), 7.16–7.18 (d, J = 8.28 Hz, 1H, ArH), 7.43–7.46 (dd, J = 8.36 Hz, 1.88 Hz, 1H, ArH), 7.52–7.54 (d, J = 8.44 Hz, 1H, ArH), 7.58 (s, 1H, 1H, ArH), 8.08 (d, J = 1.84 Hz, 1H, ArH), 8.66 (s, 1H, N═C-H), 10.96 (s, 1H, NH) ppm; ^{13}C NMR (100 MHz, DMSO-d_6): δ = 55.25, 55.78, 109.60, 111.81, 112.31, 117.81, 124.84, 125.75, 125.96, 125.33, 132.73, 143.51, 149.14, 150.39, 152.87, 163.43, 164.45 ppm.

4.2.11. (Z)-5-chloro-3-(((E)-pyridin-3-ylmethylene)hydrazono)indolin-2-one (4k)

Crimson red solid; Yield: 73%; mp: 287–289 °C; FTIR (ATR, ν_{max}, cm^{-1}): 1455 (Aromatic C═C stretch), 1552 (N—H bend), 1612 (C═O), 1736 (C═N), 3155 (N—H stretch); ^{1}H NMR (400 MHz, DMSO-d_6): δ = 6.90–6.92 (d, J = 8.40 Hz, 1H, ArH), 7.43–7.46 (dd, J = 8.38 Hz, 2.18 Hz, 1H, ArH), 7.61–7.64 (m, 1H, ArH), 8.32–8.35 (m, 1H, ArH), 8.70 s, 1H, N═C-H), 8.75–8.76 (d, J = 4.82, 1.52 Hz, 1H, ArH), 11.02 (s, 1H, NH) ppm; ^{13}C NMR (100 MHz, DMSO-d_6): δ = 112.47, 117.33, 124.38, 125.87, 128.04, 129.05, 133.30, 135.21, 143.91, 149.85, 150.22, 152.60, 158.89, 164.00.

4.2.12. (Z)-5-chloro-3-(((E)-thiophen-2-ylmethylene)hydrazono)indolin-2-one (4 l)

Crimson red solid; Yield: 69%; mp: 253–255 °C; FTIR (ATR, ν_{max}, cm^{-1}): 1440 (Aromatic C═C stretch), 1504 (N—H bend), 1603 (C═O), 1722 (C═N), 3088 (N—H stretch); ^{1}H NMR (400 MHz, DMSO-d_6): δ = 6.82–6.84 (d, J = 8.32 Hz, 1H, ArH), 7.21–7.24 (dd, J = 4.94 Hz, 3.70 Hz, 1H, ArH), 7.36–7.39 (dd, J = 8.36 Hz, 2.20 Hz, 1H, ArH), 7.74–7.75 (dd, J = 3.84 Hz, 0.76 Hz, 1H, ArH), 7.92–7.94 (d, J = 5.03 Hz, 1H, ArH), 7.97–7.98 (d, J = 2.20 Hz, 1H, ArH), 8.90 (s, 1H, N═C-H), 10.89 (s, 1H, NH) ppm; ^{13}C NMR (100 MHz, DMSO-d_6): δ = 112.34, 117.79, 125.81, 128.41, 129.00, 132.94, 133.86, 136.13, 138.26, 143.68, 150.87, 158.6, 164.37 ppm.

4.2.13. (Z)-5-chloro-3-(((E)-furan-2-ylmethylene)hydrazono)indolin-2-one (4 m)

Brown solid; Yield: 70%; mp: 204–206 °C; FTIR (ATR, ν_{max}, cm^{-1}): 1458 (Aromatic C═C stretch), 1534 (N—H bend), 1616 (C═O), 1741 (C═N), 3152 (N—H stretch); ^{1}H NMR (400 MHz, DMSO-d_6): δ = 6.81–6.82 (m, 2H, ArH), 6.90–6.92 (d, J = 8.40 Hz, 1H, ArH), 7.36–7.37 (d, J = 3.48 Hz, 1H, ArH), 7.44–7.47 (dd, J = 8.36 Hz, 2.24 Hz, 1H, ArH), 8.09–8.15 (m, 2H, ArH), 8.61 (s, 1H, N═C-H), 10.97 (s, NH), ppm; ^{13}C NMR (100 MHz, DMSO-d_6): δ = 112.31, 113.34, 117.83, 121.00, 125.79, 128.27, 133.00, 143.61, 148.61, 148.83, 150.83, 152.30, 164.35 ppm.

4.2.14. (Z)-3-(((E)-(5-nitrothiophen-2-yl)methylene)hydrazono)indolin-2-one (4n)

Reddish brown solid; Yield: 68%; mp: 222–224 °C; FTIR (ATR, ν_{max}, cm^{-1}): 1450 (Aromatic C═C stretch), 1529 (N—H bend), 1607 (C═O), 1738 (C═N), 3102 (N—H stretch); ^{1}H NMR (400 MHz, DMSO-d_6): δ = 6.92–6.94 (d, J = 4.28 Hz, 1H, ArH), 7.48–7.49 (d, J = 2.20 Hz, 1H, ArH), 7.79–7.82 (m, 2H, ArH), 8.94 (s, 1H, N═C-H), 10.09 (s, 1H, NH); ^{13}C NMR (100 MHz, DMSO-d_6): δ = 112.60, 117.06, 117.32, 126.09, 128.35, 130.53, 133.68, 133.91, 144.25, 145.90, 149.03, 151.29, 156.32, 163.23 ppm.

4.2.15. (Z)-5-chloro-3-(((E)-pyridin-4-ylmethylene)hydrazono)indolin-2-one (4o)

Brown solid; Yield: 71%; mp: 272–274 °C; FTIR (ATR, ν_{max}, cm^{-1}): 1419 (Aromatic C═C stretch), 1554 (N—H bend), 1614 (C═O), 1734 (C═N), 3157 (N—H stretch); ^{1}H NMR (400 MHz, DMSO-d_6): δ = 6.85–6.87 (d, J = 8.36 Hz, 1H, ArH), 7.39–7.42 (dd, J = 8.36 Hz, 2.24 Hz, 1H, ArH), 7.55–7.56 (d, J = 2.28 Hz, 1H, ArH), 7.77–7.78 (m, 2H, ArH), 8.48 (s, 1H, , N═C-H), 8.73–8.74 (m, 2H, ArH), 10.98 (s, 1H, NH) ppm; ^{13}C NMR (100 MHz, DMSO-d_6): δ = 112.62, 117.14, 121.93, 125.90, 127.80, 133.52, 139.92, 144.04, 148.74, 150.80, 156.80, 163.73 ppm.

4.3. General procedure for the synthesis of 3-(((E)-arylidene) hydrazono)-1-(thiomorpholinomethyl)indolin-2-one 5(a-o)

In a round bottom flask, 3-arylidinehydrazonoindoline-2one **4(a-o)** (1 mmol), formaldehyde (1.2 mmol) and ethanol (10 ml) were added and stirred at room temperature for 10 min. Thiomorpholine (1.2 mmol) was added to the reaction mixture and continued the stirring for additional 3 h at room temperature. Upon completion of the reaction (as monitored by TLC), the formed precipitate was filtered, washed with ethanol followed by diethyl ether and dried to obtain the 3-(((*E*)-arylidene)hydrazono)-1-(thiomorpholino-methy)indolin-2-ones **5(a-o)** in excellent yields.

4.3.1. (Z)-3-(((E)-4-methoxybenzylidene)hydrazono)-1-(thiomorpholino-methyl)indolin-2-one (5a)

Yellow solid; Yield: 83%; mp: 137–139 °C; FTIR (ATR, ν_{max}, cm^{-1}): 1457 (Aromatic C═C stretch), 1600 (C═O), 1717 (C═N); ^{1}H NMR (400 MHz, DMSO-d_6): δ = 2.57–2.59 (t, J = 4.88 Hz, 4H), 2.82–2.84 (t, J = 4.88 Hz, 4H), 3.86 (s, 3H, –OCH_3), 4.49 (s, 2H, –CH_2-), 7.12–7.14 (d, J = 8.64 Hz, 3H, ArH), 7.22–7.24 (d, J = 7.92 Hz, 1H, ArH), 7.45–7.49 (m, 1H, ArH), 7.95–7.97 (d, J = 8.72 Hz, 2H, ArH), 8.10–8.12 (d, J = 7.36 Hz, 1H, ArH), 8.65 (s, 1H, -N = CH) ppm; ^{13}C NMR (100 MHz, DMSO-d_6): δ = 26.93, 52.18, 55.52, 62.06, 110.96, 114.78, 116.01, 122.92, 125.97, 128.51, 131.11, 133.24, 145.76, 149.76, 162.28, 162.70, 164.28 ppm; HRMS (ESI) *m/z* calcd. for $C_{22}H_{22}N_4O_2S$, 394.1463: found 417.1361 [M + Na] $^+$

4.3.2. (Z)-3-(((E)-3,4-dimethoxybenzylidene)hydrazono)-1-(thiomorpholino-methyl)indolin-2-one (5b)

Crimson red solid; Yield: 72%; mp: 121–123 °C; FTIR (ATR, ν_{max}, cm^{-1}): 1466 (Aromatic C═C stretch), 1604 (C═O), 1718 (C═N); ^{1}H NMR (400 MHz, DMSO-d_6): δ = 2.56–2.59 (t, J = 4.96 Hz, 4H), 2.82–2.84 (t, J = 5.02 Hz, 4H), 3.86 (s, 3H, –OCH_3), 3.87 (s, 3H, –OCH_3), 4.49 (s, 2H, –CH_2-), 7.10–7.16 (m, 2H, ArH), 7.12–7.24 (d, J = 7.92 Hz, 1H, ArH), 7.46–7.48 (m, 1H, ArH), 7.54–7.57 (m, 2H, ArH), 8.06–8.08 (d, J = 7.36 Hz, 1H, ArH), 8.59 (s, 1H, -N = CH) ppm; ^{13}C NMR (100 MHz, DMSO-d_6): δ = 26.93, 52.18, 55.49, 55.73, 62.06, 110.37, 110.90, 111.77, 115.96, 122.95, 124.10, 126.05, 128.43, 133.20, 145.74, 149.11, 149.54, 152.58, 161.77, 164.25 ppm; HRMS (ESI) *m/z* calcd. for $C_{22}H_{24}N_4O_3S$, 424.1569: found 447.1470 [M + Na] $^+$

4.3.3. (Z)-3-(((E)-pyridin-3-ylmethylene)hydrazono)-1-(thiomorpholino-methyl)-indolin-2-one (5c)

Yellow solid; Yield: 72%; mp: 175–177 °C; FTIR (ATR, ν_{max}, cm^{-1}): 1468 (Aromatic C═C stretch), 1599 (C═O), 1724 (C═N); ^{1}H NMR (400 MHz, DMSO-d_6): δ = 2.57–2.59 (t, J = 5.00 Hz, 4H), 2.82–2.85 (t, J = 5.02 Hz, 4H), 4.50 (s, 2H, –CH_2-), 7.10–7.14 (t, J = 7.56 Hz, 1H, ArH), 7.24–7.26 (d, J = 7.92 Hz, 1H, ArH), 7.47–7.51 (m, 1H, ArH), 7.60–7.63 (dd, J = 7.90 Hz, 4.82 Hz, 1H, ArH), 7.91–7.93 (d, J = 7.48 Hz, 1H, ArH), 8.37–8.40 (m, 1H, ArH), 8.68 (s, 1H, -N = CH), 8.68–8.76 (m, 1H, ArH), 9.09–9.10 (d, J = 1.84 Hz, 1H, ArH) ppm; ^{13}C NMR (100 MHz, DMSO-d_6): δ = 26.93, 52.16, 62.13, 11.08, 115.62, 123.10, 124.35, 128.58, 129.15, 133.73, 135.26, 146.10, 149.40, 150.25, 152.45, 157.61, 163.91 ppm; HRMS (ESI) *m/z* calcd. for $C_{19}H_{19}N_5OS$, 365.1310: found 388.1210 [M + Na] $^+$

4.3.4. (Z)-1-(thiomorpholinomethyl)-3-(((E)-thiophen-2-ylmethylene)-hydrazono)-indolin-2-one (5d)

Pale red solid; Yield: 74%; mp: 186–188 °C; FTIR (ATR, ν_{max}, cm^{-1}): 1460 (Aromatic C═C stretch), 1605 (C═O), 1714 (C═N); ^{1}H NMR (400 MHz, DMSO-d_6): δ = 2.56–2.59 (t, J = 5.08 Hz, 4H), 2.81–2.84 (t, J = 4.95 Hz, 4H), 4.49 (s, 2H, –CH_2-), 7.11–7.15 (t, J = 7.58 Hz, 1H, ArH), 7.22–7.24 (d, J = 7.88 Hz, 1H, ArH), 7.28–7.30 (m, 1H, ArH), 7.45–7.49 (m, 1H, ArH), 7.80–7.81 (d, J = 3.20 Hz, 1H, ArH), 7.97–7.98 (d, J = 5.00 Hz, 1H, ArH), 8.07–8.09 (d, J = 7.36 Hz, 1H, ArH), 8.94 (s, 1H -N = CH) ppm; ^{13}C NMR (100 MHz, DMSO-d_6): δ = 26.94, 52.16, 62.07, 111.01, 116.03, 122.89, 128.56, 128.90, 133.39, 133.46, 135.54, 138.36, 145.94, 150.39, 157.40, 164.21 ppm; HRMS (ESI) *m/z* calcd. for $C_{18}H_{18}N_4O_3S_2$, 370.0922: found 393.0820 [M + Na] $^+$

4.3.5. (Z)-3-(((E)-furan-2-ylmethylene)hydrazono)-1-(thiomorpholinomethyl)-indolin-2-one (5e)

Yellow solid; Yield: 72%; mp: 174–176 °C; FTIR (ATR, ν_{max}, cm^{-1}): 1462 (Aromatic C═C stretch), 1628 (C═O), 1720 (C═N); ^{1}H NMR (400 MHz, DMSO-d_6): δ = 2.56–2.59 (t, J = 5.16 Hz, 4H), 2.81–2.84 (t, J = 4.95 Hz, 4H), 4.49 (s, 2H, –CH_2-), 6.80–6.81 (m, 1H, ArH), 7.10–7.14 (t, J = 7.60 Hz, 1H, ArH), 7.22–7.24 (d, J = 7.92 Hz, 1H, ArH), 7.35–7.36 (d, J = 3.48 Hz, 1H, ArH), 7.45–7.49 (m, 1H, ArH), 8.10–8.15 (m, 2H, ArH), 8.57 (s, 1H, -N = CH) ppm; ^{13}C NMR (100 MHz, DMSO-d_6): δ = 26.93, 52.17, 62.08, 110.93, 113.22, 116.07, 120.06, 122.89, 128.66, 133.45, 145.84, 148.21, 148.99, 150.39, 151.07, 164.19 ppm; HRMS (ESI) *m/z* calcd. for $C_{18}H_{18}N_4O_2S$, 354.1150: found 377.1051 [M + Na] $^+$

4.3.6. (Z)-3-(((E)-(5-nitrothiophen-2-yl)methylene)hydrazono)-1-(thiomorpholino-methyl)indolin-2-one (5f)

Brick red solid; Yield: 75%; mp: 188–189 °C; FTIR (ATR, ν_{max}, cm^{-1}): 1456 (Aromatic C═C stretch), 1609 (C═O), 1724 (C═N); ^{1}H NMR (400 MHz, DMSO-d_6): δ = 2.57–2.59 (t, J = 5.00 Hz, 4H), 2.81–2.84 (t, J = 4.64 Hz, 4H), 4.49 (s, 2H, –CH_2-), 7.14–7.18 (t, J = 7.64 Hz, 1H, ArH), 7.24–7.26 (d, J = 7.96 Hz, 1H, ArH), 7.49–7.53 (t, J = 7.40 Hz, 1H, ArH), 7.79–7.85 (m, 2H, ArH), 8.21 (s, 1H, ArH), 8.90 (s, 1H, -N = CH) ppm; ^{13}C NMR (100 MHz, DMSO-d_6): δ = 26.94, 52.13, 62.17, 111.27, 115.72, 123.19, 128.62, 129.12, 130.51, 133.35, 134.18, 134.40, 136.42, 146.45, 153.47, 154.53 ppm; HRMS (ESI) *m/z* calcd. for $C_{18}H_{17}N_5O_3S_2$, 415.0773: found 438.0672 [M + Na] $^+$

4.3.7. (Z)-3-(((E)-pyridin-4-ylmethylene)hydrazono)-1-(thiomorpholinomethyl) indolin-2-one (5 g)

Crimson red solid; Yield: 79%; mp: 222–224 °C; FTIR (ATR, ν_{max}, cm^{-1}): 1463 (Aromatic C═C stretch), 1599 (C═O), 1724 (C═N); ^{1}H NMR (400 MHz, DMSO-d_6): δ = 2.57–2.59 (t, J = 5.00 Hz, 4H), 2.82–2.85 (t, J = 5.04 Hz, 4H), 4.50 (s, 2H, –CH_2-), 7.08–7.12 (t, J = 7.60 Hz, 1H, ArH), 7.24–7.26 (d, J = 7.92 Hz, 1H, ArH), 7.47–7.51 (m, 1H, ArH), 7.74–7.76 (d, J = 7.32 Hz, 1H, ArH), 7.87–7.88 (m, 2H, ArH), 8.51 (s, 1H, -N = CH), 8.79–8.80 (m, 2H, ArH) ppm; ^{13}C NMR (100 MHz, DMSO-d_6): δ = 26.94, 52.15, 62.16, 111.18, 115.41, 122.04, 123.09, 128.29, 133.89, 140.05, 146.22, 148.32, 150.71, 155.77, 163.64 ppm; HRMS (ESI) *m/z* calcd. for $C_{19}H_{19}N_5OS$, 365.1310: found 388.1209[M + Na] $^+$

4.3.8. (Z)-3-(((E)-(5-nitrofuran-2-yl)methylene)hydrazono)-1-(thiomorpholino-methyl)indolin-2-one (5 h)

Crimson red solid; Yield: 68%; mp: 195–197 °C; FTIR (ATR, ν_{max}, cm^{-1}): 1463 (Aromatic C═C stretch), 1628 (C═O), 1721 (C═N); ^{1}H NMR (400 MHz, DMSO-d_6): δ = 2.57–2.59 (t, J = 4.96 Hz, 4H), 2.82–2.85 (t, J = 5.02 Hz, 4H), 4.50 (s, 2H, –CH_2-), 7.09–7.13 (t, J = 7.78 Hz, 1H, ArH), 7.24–7.26 (d, J = 7.92 Hz, 1H, ArH), 7.49–7.53 (m, 1H, ArH), 7.56–7.57 (d, J = 3.96 Hz, 1H, ArH), 7.86–7.87 (d, J = 3.96 Hz, 1H, ArH), 7.89–7.91 (dd, J = 7.52 Hz, 0.76 Hz, 1H, ArH), 8.58 (s, 1H, -N = CH) ppm; ^{13}C NMR (100 MHz, DMSO-d_6): δ = 26.93, 52.15, 62.20, 111.18, 114.15, 115.56, 1119.25, 123.07, 128.70, 134.14, 146.34, 147.31, 149.52, 150.17, 152.90, 163.72 ppm; HRMS (ESI) *m/z* calcd. for $C_{18}H_{17}N_5O_4S$, 399.1001: found 400.1080 [M + H] $^+$

4.3.9. (Z)-5-chloro-3-(((E)-4-methoxybenzylidene)hydrazono)-1-(thiomorpholinomethyl)indolin-2-one (5i)

Yellow solid; Yield: 82%; mp: 205–207 °C; FTIR (ATR, ν_{max}, cm^{-1}): 1458 (Aromatic C═C stretch), 1625 (C═O), 1733 (C═N); ^{1}H NMR (400 MHz, DMSO-d_6): δ = 2.56–2.57 (d, J = 4.00 Hz, 4H), 2.81–2.82 (d, J = 4.72 Hz, 4H), 3.87 (s, 3H, –OCH_3), 4.49 (s, 2H, –CH_2-), 7.16–7.18 (d, J = 8.52 Hz, 1H, ArH), 7.25–7.28 (d, J = 8.64 Hz, 1H, ArH), 7.52–7.55 (dd, J = 8.42 Hz, 1.54 Hz, 1H, ArH), 7.93–7.95 (d, J = 8.52 Hz, 1H, ArH), 8.05–8.06 (d, J = 1.40 Hz, 1H, ArH), 8.70 (s, 1H, -N = CH) ppm; ^{13}C NMR (100 MHz, DMSO-d_6): δ = 26.91, 52.07, 55.59, 62.18, 112.62, 114.94, 117.20, 125.75, 126.56, 127.67, 127.89, 131.19, 132.52, 144.45, 149.05, 163.00, 163.68 ppm; HRMS (ESI) *m/z* calcd. for $C_{21}H_{21}ClN_4O_2S$, 428.1074: found 451.0972 [M + Na] $^+$

4.3.10. (Z)-5-chloro-3-(((E)-3,4-dimethoxybenzylidene)hydrazono)-1-(thiomorpholino- methyl)indolin-2-one (5j)

yellow solid; Yield: 80%; mp: 210–212 °C; FTIR (ATR, ν_{max}, cm^{-1}): 1458 (Aromatic C═C stretch), 1599 (C═O), 1731 (C═N); ^{1}H NMR (400 MHz, DMSO-d_6): δ = 2.57 (s, 4H), 2.81 (s, 4H), 3.87 (s, 6H, –OCH_3), 4.47 (s, 2H, –CH_2-), 6.85 (s, 1H, ArH), 7.16 (s, 1H, ArH), 7.50–7.56 (d, 2H, ArH), 8.23 (s, 2H, ArH), 8.65 (s, 1H, -N = CH) ppm; ^{13}C NMR (100 MHz, DMSO-d_6): δ = 26.91, 52.07, 55.59, 62.18, 112.62, 114.94, 117.20, 125.75, 126.56, 127.67, 127.89, 131.19, 132.52, 144.45, 149.05, 163.00, 163.68 ppm; HRMS (ESI) *m/z* calcd. for $C_{22}H_{23}ClN_4O_3S$, 458.1179: found 481.1080[M + Na] $^+$

4.3.11. (Z)-5-chloro-3-(((E)-pyridin-3-ylmethylene)hydrazono)-1-(thiomorpholinomethyl)-indolin-2-one (5 k)

Pale red solid; Yield: 75%; mp: 192–194 °C; FTIR (ATR, ν_{max}, cm^{-1}): 1458 (Aromatic C═C stretch), 1602 (C═O), 1723 (C═N); ^{1}H NMR (400 MHz, DMSO-d_6): δ = 2.57 (s, 4H), 2.82 (s, 4H), 4.48 (s, 2H, –CH_2-), 7.08–7.12 (t, J = 7.56 Hz, 1H, ArH), 7.23–7.25 (d, J = 7.87 Hz, 1H, ArH), 7.48–7.56 (m, 2H, ArH), 7.25–7.90 (m, 2H, ArH), 8.57 (s, 1H, -N = CH) ppm: ^{13}C NMR (100 MHz, DMSO-d_6): δ = 26.91, 52.06, 62.20, 112.88, 117.31, 120.98, 121.31, 125.80, 126.60, 128.27, 132.99, 144.51, 149.16, 152.53, 164.51, 178.37 ppm; HRMS (ESI) *m/z* calcd. for $C_{19}H_{18}ClN_5OS$, 399.0921: found 422.0819 [M + Na] $^+$

4.3.12. (Z)-5-chloro-1-(thiomorpholinomethyl)-3-(((E)-thiophen-2-yl-methylene)-hydrazono)-indolin-2-one (5 l)

Yellow solid; Yield: 72%; mp: 202–204 °C; FTIR (ATR, ν_{max}, cm^{-1}): 1440 (Aromatic C═C stretch), 1627 (C═O), 1722 (C═N); ^{1}H NMR (400 MHz, DMSO-d_6): δ = 2.56–2.58 (t, J = 4.76 Hz, 4H), 2.80–2.82 (t, J = 4.76 Hz, 4H), 4.48 (s, 2H, –CH_2-), 7.25–7.27 (d, J = 8.48 Hz, 2H, ArH), 7.30–7.32 (m, 1H, ArH), 7.53–7.55 (dd, J = 8.48 Hz, 2.20 Hz, 1H, ArH), 7.84–7.85 (d, J = 3.28 Hz, 1H, ArH), 8.02–8.03 (d, J = 4.96 Hz, 1H, ArH), 8.11–8.12 (d, J = 2.12 Hz, 1H, ArH), 9.01 (s, 1H, -N = CH) ppm; ^{13}C NMR (100 MHz, DMSO-d_6): δ = 27.43, 52.64, 62.79, 113.07, 117.87, 127.27, 128.62, 129.41, 133.12, 134.24, 136.28, 138.80, 145.07, 150.21, 158.57, 164.32 ppm; HRMS (ESI) *m/z* calcd. for $C_{18}H_{17}ClN_4OS_2$, 404.0532: found 427.0432 [M + Na] $^+$

4.3.13. (Z)-5-chloro-3-(((E)-furan-2-ylmethylene)hydrazono)-1-(thiomorpholino-methyl)-indolin-2-one (5 m)

Brick red solid; Yield: 68%; mp: 189–191 °C; FTIR (ATR, ν_{max}, cm^{-1}): 1434 (Aromatic C═C stretch), 1634 (C═O), 1731 (C═N); ^{1}H NMR (400 MHz, DMSO-d_6): δ = 2.57–2.58 (d, J = 4.88 Hz, 4H), 2.80–2.82 (d, J = 5.28 Hz, 4H), 4.48 (s, 2H, –CH_2-), 6.82–6.83 (m, 1H, ArH), 7.25–7.27 (d, J = 8.52 Hz, 1H, ArH), 7.38–7.39 (d, J = 3.40 Hz, 1H, ArH), 7.53–7.55 (dd, J = 8.46 Hz, 2.14 Hz, 1H, ArH), 8.16 (d, J = 1.28 Hz, 2H, ArH), 8.63 (s, 1H, -N = CH) ppm; ^{13}C NMR (100 MHz, DMSO-d_6): δ = 26.90, 52.06, 62.20,112.62, 113.41, 117.31, 121.32, 126.60, 127.92, 132.73, 144.52, 148.76, 148.80, 149.88, 152.51, 163.88 ppm; HRMS (ESI) *m/z* calcd. for $C_{18}H_{17}ClN_4O_2S$, 388.0761: found 411.0659 [M + Na] $^+$

4.3.14. (Z)-5-chloro-3-(((E)-(5-nitrothiophen-2-yl)methylene) hydrazono)-1-(thiomorpholino-methyl)indolin-2-one (5n)

Brown solid; Yield: 79%; mp: 206–208 °C; FTIR (ATR, ν_{max}, cm^{-1}): 1438 (Aromatic C═C stretch), 1604 (C═O), 1728 (C═N); ^{1}H NMR (400 MHz, DMSO-d_6): δ = 2.56–2.58 (d, J = 5.0 Hz, 4H), 2.80–2.83 (d, J = 4.95 Hz, 4H), 4.48 (s, 2H, –CH_2-), 6.82–6.83 (m, 1H, ArH), 7.25–7.27 (d, J = 8.52 Hz, 1H, ArH), 7.38–7.39 (d, J = 3.48 Hz, 1H, ArH), 7.53–7.56 (dd, J = 8.48 Hz, 2.32 Hz, 1H, ArH), 8.16–8.17 (d, J = 1.88 Hz, 2H, ArH), 8.64 (s, 1H, -N = CH) ppm; ^{13}C NMR (100 MHz, DMSO-d_6): δ = 26.91, 52.05, 62.20, 112.62, 113.41, 117.31, 121.34, 126.59, 127.92, 127.92, 132.72, 144.52, 148.72, 148.80, 149.89, 152.54, 163.88 ppm; HRMS (ESI) *m/z* calcd. for $C_{18}H_{16}ClN_5O_3S_2$, 449.0383: found 472.0283

$[M + Na]^+$

4.3.15. (Z)-5-chloro-3-(((E)-pyridin-4-ylmethylene)hydrazono)-1-(thiomorpholino-methyl)-indolin-2-one (5o)

Yellow solid; Yield: 79%; mp: 194–196 °C; FTIR (ATR, ν_{max}, cm^{-1}): 1466 (Aromatic C═C stretch), 1604 (C═O), 1718 (C═N); ^{1}H NMR (400 MHz, DMSO-d_6): δ = 2.58 (s, 4H), 2.84 (s, 4H), 4.49 (s, 2H, –CH_2-), 7.09–7.13 (m, 1H, ArH), 7.24–7.26 (d, J = 7.92 Hz, 1H, ArH), 7.49–7.52 (m, 1H, ArH), 7.56–7.57 (d, J = 3.80 Hz, 1H, ArH), 7.86–7.87 (d, J = 3.68 Hz, 1H, ArH), 7.89–7.91 (d, J = 7.60 Hz, 1H, ArH), 8.58 (s, 1H, -N = CH) ppm; ^{13}C NMR (100 MHz, DMSO-d_6): δ = 26.93, 52.15, 62.20, 111.17, 114.14, 115.56, 119.24, 123.06, 128.69, 134.13, 146.33, 147.31, 149.53, 15017, 152.89, 163.71 ppm; HRMS (ESI) *m/z* calcd. for $C_{19}H_{18}ClN_5OS$, 399.0921: found 422.0819 $[M + Na]^+$

4.4. Biological studies

4.4.1. Anti-mycobacterial evaluation (MIC) under aerobic conditions by in vitro

All the newly synthesized compounds **4(a-o)** and **5(a-o**) were screened for their *in vitro* anti-mycobacterial activity against *M. tuberculosis* H_{37}Rv grown under aerobic conditions using a dual readout (OD_{590} and fluorescence) assay procedure [41,42,53]. The experiment was carried out at Infectious Disease Research Institute (IDRI) within the National Institute of Allergy and Infectious Diseases (NIAID) screening program, Bethesda, MD, USA. Test compounds were prepared as 10-point two-fold serial dilutions in DMSO and diluted into 7H9-Tw-OADC medium in 96-well plates with a final DMSO concentration of 2%. The highest concentration of compound was 200 μM and compounds were soluble in DMSO at 10 mM. For compounds with limited solubility, the highest concentration was 50X less than the stock concentration e.g. 100 μM for 5 mM DMSO stock, 20 μM for 1 mM DMSO stock. For potent compounds, assays were repeated at lower starting concentrations. Each plate included assay controls for background (medium/DMSO only, no bacterial cells), zero growth (100 μM Rifampicin) and maximum growth (DMSO only), as well as a rifampicin dose response curve (DRC). Plates were inoculated with *M. tuberculosis* and incubated for 5 days. Growth was measured by OD_{590} and fluorescence (Ex_{560}/Em_{590}) using a Bio-Tek™ Synergy4 plate reader and calculated separately for OD_{590} and RFU. MIC was determined on the basis of 10-point dose response curve which was plotted as % growth. The MIC was defined as the minimum concentration at which growth was completely inhibited and was calculated from the inflection point of the fitted curve to the lower asymptote (zero growth). In addition, DRC were generated using the Levenberg-Marquardt algorithm and the concentrations that resulted in 50% and 90% inhibition of growth were determined (IC_{50} and IC_{90}, respectively).

4.4.2. MIC determination under hypoxic (low) oxygen condition [46]

Test compounds (**4f**, **4 h**, **4n**, **5f**, and **5 m**) were prepared as 20-point two-fold serial dilutions in DMSO and diluted into DTA medium in 96-well plates to a final DMSO concentration of 2%. The highest concentration of compound was 200 μM where compounds were soluble in DMSO at 10 mM. For compounds with limited solubility, the highest concentration was 50X less than the stock concentration e.g. 100 μM for 5 mM DMSO stock, 20 μM for 1 mM DMSO stock. Control compounds were prepared as two-fold serial dilutions in DMSO and diluted into DTA medium in 96-well plates with a final DMSO concentration of 2%. MTB constitutively expressing the luxABCDE operon was inoculated into DTA medium in gas-impermeable glass tubes and incubated for 18 days to generate hypoxic conditions (Wayne model of hypoxia). At this point, bacteria are in a non-replicating state (NRP stage 2) induced by oxygen depletion. Oxygen-deprived bacteria were inoculated into compound assay plates and incubated under anaerobic conditions for 10 days followed by incubation under aerobic conditions (outgrowth) for 28 h. Oxygen-deprived bacteria were also inoculated into compound assay plates and incubated under aerobic conditions for 5 days. Growth was measured by luminescence. Rifampicin was included in each plate and metronidazole was included in each run as positive controls for aerobic and anaerobic killing of MTB, respectively.

4.4.3. Minimum bactericidal concentration (MBC) determination

MTB was grown aerobically to logarithmic phase and inoculated into liquid medium containing four different compound concentrations with a final maximum concentration of 2% DMSO. For test compounds (**4f**, **4 h**, **4n**, **5f**, and **5 m**) with MIC < 20 μM, the concentration selected were 10X MIC, 5X MIC, 1X MIC and 0.25X MIC. Cultures were exposed to compounds for 21 days and cell viability measured by enumerating colony forming units on agar plates on day 0, 7, 14 and 21. MBC was defined as the minimum concentration required to achieve a 2-log kill in 21 days. For compounds with > 1-log kill, an assessment of time and/or concentration-dependence was determined from the kill kinetics. DMSO was used as a positive control for growth.

4.4.4. Intracellular activity evaluation [47]

The activity of compounds against intracellular bacteria was determined by measuring viability in infected THP-1 cell after 3 days in the presence of test compounds. Test compounds (**4f**, **4 h**, **4n**, **5f**, and **5 m**) were prepared as 10-point three-fold serial dilutions in DMSO. The highest concentration of compound tested was 50 μM where compounds were soluble in DMSO at 10 mM. For compounds with limited solubility, the highest concentration was 200X less than the stock concentration e.g. 25 μM for 5 mM DMSO stock, 5 μM for 1 mM DMSO stock. THP-1 cells were cultured incomplete RPMI and differentiated into macrophage-like cells using 80 nM PMA overnight at 37 °C, 5% CO_2. THP-1 cells were infected with a luminescent strain of H_{37}Rv (which constitutively expresses luxABCDE) at a multiplicity of infection of THP-1 and incubated over night at 37 °C, 5% CO_2. Infected cells were recovered using Accutase/EDTA solution, washed twice with PBS to remove extracellular bacteria and seeded into assay plates. Compound dilutions were added to a final DMSO concentration of 0.5%. Assay plates were incubated for 72 h at 37 °C, 5% CO_2. Each run included isoniazid as a control. Relative luminescent units (RLU) were measured using a Biotek Synergy 2 plate reader. The dose response curve was fitted using the Levenberg–Marquardt algorithm. The IC_{50} and IC_{90} were defined as the compound concentrations that produced 50% and 90% inhibition of growth, respectively.

4.4.5. Cytotoxicity assay [47]

The cytotoxicity of compounds was determined by measuring THP-1 cell viability after 3 days in the presence of test compounds. Test compounds (**4f**, **4 h**, **4n**, **5f**, and **5 m**) were prepared as 10-point three-fold serial dilutions in DMSO. The highest concentration of compound tested was 50 μM where compounds were soluble in DMSO at 10 mM. For compounds with limited solubility, the highest concentration was 200X less than the stock concentration e.g. 25 μM for 5 mM DMSO stock, 5 μM for 1 mM DMSO stock. Each plate included staurosporine as a control. THP-1 cells were cultured incomplete RPMI and differentiated into macrophage-like cells using 80 nM PMA overnight at 37 °C, 5% CO_2. Cells were inoculated into assay plates and cultured for 24 h before compound dilutions were added to a final DMSO concentration of 0.5%. Each run included staurosporine as a control. Assay plates were incubated for 3 days at 37 °C, 5% CO_2; growth was measured using the CellTiter-Glo® Luminescent Cell Viability Assay (Promega) which uses ATP as an indicator of cell viability. Relative luminescent units (RLU) were measured using a Biotek Synergy 4 plate reader. The DRC was fitted using the Levenberg–Marquardt algorithm. The IC_{50} was defined as the compound concentration that produced 50% inhibition of growth.

4.4.6. MIC determination against drug-resistant isolates of M. Tuberculosis [42]

The MIC of compound was determined by measuring bacterial

growth after 5 days in the presence of test compounds. Test compounds (**4f**, **4 h**, **4n**, **5f**, and **5 m**) were prepared as 10-point two-fold serial dilutions in DMSO and diluted into 7H9-Tw-OADC medium in 96-well plates with a final DMSO concentration of 2%. The highest concentration of compound was 200 μM where compounds were soluble in DMSO at 10 mM. For compounds with limited solubility, the highest concentration was 50X less than the stock concentration e.g. 100 μM for 5 mM DMSO stock, 20 μM for 1 mM DMSO stock. Each plate included assay controls for background (medium/DMSO only, no bacterial cells), zero growth (100 μM rifampicin) and maximum growth (DMSO only), as well as a DRC of rifampicin. Plates were inoculated with drug-resistant isolates of MTB and incubated for 5 days and growth was measured by OD_{590}. To calculate the MIC, the 10-point DRC was plotted as % growth and fitted to the Gompertz model using GraphPad Prism 5. The MIC was defined as the minimum concentration at which growth was completely inhibited and was calculated from the inflection point of the fitted curve to the lower asymptote (zero growth). In addition dose response curves were generated using the Levenberg-Marquardt algorithm and the concentrations that resulted in 50% (IC_{50}) and 90% (IC_{90}) inhibition of growth were determined, respectively.

4.4.7. *MIC determination against other disease-relevant mycobacterial species [42,47]*

The MIC values was determined by measuring bacterial growth in the presence of test compounds. Test compounds (**4f**, **4 h**, **4n**, **5f**, and **5 m**) were prepared as 20-point two-fold serial dilutions in DMSO and diluted into 7H9-Tw-OADC medium in 96-well plates with a final DMSO concentration of 2%. The highest concentration of compound was 200 μM where compounds were soluble in DMSO at 10 mM. For compounds with limited solubility, the highest concentration was 50X less than the stock concentration e.g. 100 μM for 5 mM DMSO stock, 20 μM for 1 mM DMSO stock. Each plate included assay controls for background (medium/DMSO only, no bacterial cells), zero growth (100 μM rifampicin) and maximum growth (DMSO only), as well as DRC of rifampicin.

4.4.7.1. Mycobacterium abscessus. Plates were inoculated with M. abscessus and incubated for 3 days at 37 ℃ and growth was measured by OD_{590}. To dose response curve was plotted as % growth and fitted to the Gompertz model. The MIC was defined as the minimum concentration at which growth was completely inhibited and was calculated from the inflection point of the fitted curve to the lower asymptote (zero growth). In addition, dose response curves were generated using the Levenberg-Marquardt algorithm and the concentrations that resulted in 50% and 90% inhibition of growth was determined (IC_{50} and IC_{90}, respectively). Rifampicin was included once in each run.

4.4.7.2. Mycobacterium avium. Plates were inoculated with M. avium, incubated for 5 days at 37 ℃ and Alamar blue was added to each well (10 μL of Alamar blue to 100 μL culture) and incubated for 24 h at 37 ℃. Plates were visually inspected and the color recorded for each well. MIC was defined as the lowest concentration at which no metabolic activity was seen (blue well).

4.5. *Computational study*

4.5.1. *Molecular docking*

We have performed docking study of all the synthesized compounds towards the GyrB ATPase domain. The ligands were prepared using LigPrep module (Schrödinger, LLC, NY, USA, 2009) by adding hydrogen atoms, removing salt, generating stereoisomers, ionizing at pH (7 ± 2) and determining valid 3D conformation [54]. Additionally, the geometry of the ligands was minimized using the standard molecular mechanic's energy function OPLS_2005 force field. The crystal structure of GyrB ATPase (PDB ID: 4B6C) was obtained from Protein Data Bank. The protein structure was prepared using the *Protein Preparation Wizard (PPrep)* module in Maestro software. Finally, the protein structure was minimized using the OPLS-2005 force field (Schrödinger, LLC, NY, USA, 2009) *Glide's Receptor Grid Generation* module was used to generate the receptor grid at the active site of co-crystalline ligand with the centered dimension cubic grid box of 10 Å × 10 Å×10 Å [55]. Finally, the low-energy conformation of the ligands was selected and docked into the grid generated from protein structures using standard precision (SP) docking mode. The evaluation was carried out with a Glide SP docking score and a single absolute best pose is produced as the output for a specific ligand [54-56].

4.5.2. *Binding free energy calculation*

Molecular mechanics with generalized born surface area (MM/GBSA) is the most popular method to estimate the ligand binding energies, which includes the OPLS3 power field and VSGB solvent model [57]. The Prime MM-GBSA simulation was carried out by using the Glide pose viewer file to calculate the total binding free energy. These poses were taken as inputs for the energy minimization of the protein–ligand complexes ($E_{complex}$), the free protein ($E_{protein}$), and the free ligands (E_{ligand}). The binding free energy ΔG_{bind} was determined according to the following equation:

▲Gbind = E. Complex (minimized) − E. ligand (minimized) − E. receptor (minimized)

The MM/GBSA calculations are used to estimate relative binding affinity of ligands to the receptor (reported in kcal/mol). As the MM/GBSA binding energies are approximate free energies of binding, a more negative value indicates stronger binding [58,59].

4.5.3. *Molecular dynamic simulations*

MD simulations for the best dock protein ligand complex was carried out using the Desmond program, an explicit solvent MD package (version 3.1, Desmond Molecular Dynamics System, Schrödinger) along with fixed optimized potentials for liquid simulation (OPLS 2005) force field [60]. The system was built up for simulation using a predefined water model (simple point charge, SPC) as solvent in an orthorhombic box with periodic boundary conditions specifying the shape and size of box as 10 Å × 10 Å × 10 Å distance. The desirable electrically neutral system for simulation was built with 0.15 M NaCl (physiological concentration of monovalent ions) in 10 Å buffer regions between the protein atoms and box sides using the system-built option. Steepest Descent and limited-memory Broyden-Fletcher Goldfarb-Shanno algorithms were applied in a hybrid manner to achieve the relaxation of the system [61]. A constant 300 K temperature and 1 atm pressure was maintained during the simulation using the Nose-Hoover thermostat algorithm and Martyna-Tobias-Klein Barostat algorithm, respectively [62]. Long-range and short-range coulombic interaction was controlled using smooth particle mesh ewald method with 9.0 Å endpoint values [62]. The simulation was achieved under NPT ensemble for 10 ns and trajectory information was obtained with the rest of 10 ps applying the Berendsen thermostat and barostat methods [62].

Supporting Information

Spectral images of all of the synthesized compounds are provided in the supporting information.

Declaration of Competing Interest

The authors declare that they have no known competing financial interests or personal relationships that could have appeared to influence the work reported in this paper.

Acknowledgments

Authors thank Discipline of Pharmaceutical Sciences, College of Health Sciences, University of KwaZulu-Natal (UKZN), South Africa (SA) for the necessary facilities. Authors sincerely thank National Institutes of Health and the National Institute of Allergy and Infectious Diseases-

Bethesda, MD, (USA) for *in vitro* anti-mycobacterial activity characterization. Authors are thankful to Inkosi Albert Luthuli central hospital, Durban, SA for antimicrobial screening and Centre for High Performance Computing-Cape Town, SA for computational resources, respectively. Author BC gratefully acknowledges National Research Foundation (NRF), SA for the research funding in the form of NRF-Innovation Post-Doctoral Research Fellowship (Grant No. 99546). RK is also thankful to NRF-SA for funding the project (Grant No. 103728 and 112079). Authors express heartfelt thanks to Mr. Dilip Jagjivan and Dr. Caryl Janse Van Rensburg (UKZN-SA) for their assistance in NMR and HR-MS experiments, respectively.

Note:

International Patent Filed: PCT Int. Appl. (2018), WO 2018100484 A1 20180607.

Appendix A. Supplementary data

Supplementary data to this article can be found online at https://doi.org/10.1016/j.bioorg.2021.105133.

References

[1] World health Organisation, Global Tuberculosis Report 2019, http://www.who.int/tb/publications/global_report/en/ (accessed July 22, 2020).
[2] Treatment for TB Disease, Cent. Dis. Control Prev. http://www.cdc.gov/tb/topic/treatment/tbdisease.htm (accessed July 22, 2020).
[3] E. Torfs, T. Piller, P. Cos, D. Cappoen, Opportunities for overcoming Mycobacterium tuberculosis drug resistance : Emerging mycobacterial targets and host-directed therapy, Int. J. Mol. Sci. 20 (2019) 2868.
[4] A. Zumla, P. Nahid, S.T. Cole, Advances in the development of new tuberculosis drugs and treatment regimens, Nat. Rev. Drug Discov. 12 (5) (2013) 388–404.
[5] R.C. Goldman, K.V. Plumley, B.E. Laughon, The evolution of extensively drug resistant tuberculosis (XDR-TB): History, status and issues for global control, Infect. Disord. Drug Targets 7 (2007) 73–91.
[6] R. Mahajan, Bedaquiline: First FDA-approved tuberculosis drug in 40 years, Int. J. Appl. Basic Med. Res. 3 (1) (2013) 1, https://doi.org/10.4103/2229-516X.112228.
[7] S. Cherukupalli, C. Balakumar, R.R. Aleti, N. Sayyad, G.A. Hampannavar, S. R. Merugu, H.R. Reddy, R. Banerjee, R. Karpoormath, Synthesis of 4,6-disubstituted pyrazolo[3,4-*d*]pyrimidine analogues: Cyclin-dependent kinase 2 (CDK2) inhibition, molecular docking and anticancer evaluation, J. Mol. Struc. 1176 (2019) 538–551.
[8] B. Chandrasekaran, S. Cherukupalli, S. Karunanidhi, A. Kajee, R.R. Aleti, N. Sayyad, B. Kushwaha, S.R. Merugu, K.P. Mlisana, R. Karpoormath, Design and synthesis of novel heterofused pyrimidine analogues as effective antimicrobial agents, J. Mol. Struct. 1183 (2019) 246–255.
[9] M. Batool, B. Ahmad, S. Choi, A structure-based drug discovery paradigm, Int. J. Mol. Sci. 20 (2019) 2783.
[10] K. Mdluli, Z. Ma, Mycobacterium tuberculosis DNA gyrase as a target for drug Discovery, Infect. Disord. Drug Targets 7 (2007) 159–168.
[11] T. Khan, K. Sankhe, V. Suvarna, A. Sherje, K. Patel, B. Dravyakar, DNA gyrase inhibitors: Progress and synthesis of potent compounds as antibacterial agents, Biomed. Pharmacother. 103 (2018) 923–938.
[12] V. Nagaraja, A.A. Godbole, S.R. Henderson, A. Maxwell, DNA topoisomerase I and DNA gyrase as targets for TB therapy, Drug Discov. Today 22 (3) (2017) 510–518.
[13] S. Petrella, E. Capton, B. Raynal, C. Giffard, A. Thureau, F. Bonneté, P.M. Alzari, A. Aubry, C. Mayer, Overall structures of Mycobacterium tuberculosis DNA gyrase reveal the role of a Corynebacteriales GyrB-specific insert in ATPase activity, Structure 27 (4) (2019) 579–589.e5.
[14] K. Chaudhari, S. Surana, P. Jain, H.M. Patel, Mycobacterium Tuberculosis (MTB) GyrB inhibitors: An attractive approach for developing novel drugs against TB, Eur. J. Med. Chem. 124 (2016) 160–185.
[15] S. Chopra, K. Matsuyama, T. Tran, J.P. Malerich, B. Wan, S.G. Franzblau, S. Lun, H. Guo, M.C. Maiga, W.R. Bishai, P.B. Madrid, Evaluation of gyrase B as a drug target in Mycobacterium tuberculosis, J. Antimicrob. Chemother. 67 (2) (2012) 415–421.
[16] P.S. Hameed, S. Suresh, M. Kakoli, et al., Optimization of pyrrolamides as mycobacterial GyrB ATPase inhibitors: structure-activity relationship and in vivo efficacy in a mouse model of tuberculosis, Antimicrob. Agents Chemother. 58 (2014) 61–70.
[17] M.C. Pirrung, S.V. Pansare, K.D. Sarma, K.A. Keith, E.R. Kern, Combinatorial optimization of isatin-β-thiosemicarbazones as anti-poxvirus agents, J. Med. Chem. 48 (8) (2005) 3045–3050.
[18] A.H. Abadi, S.M. Abou-Seri, D.E. Abdel-Rahman, C. Klein, O. Lozach, L. Meijer, Synthesis of 3-substituted-2-oxoindole analogues and their evaluation as kinase inhibitors, anticancer and antiangiogenic agents, Eur. J. Med. Chem. 41 (2006) 296–305.
[19] K. Kumar, S. Sagar, L. Esau, M. Kaur, V. Kumar, Synthesis of novel 1H–1,2,3-triazole tethered C-5 substituted uracil–isatin conjugates and their cytotoxic evaluation, Eur. J. Med. Chem. 58 (2012) 153–159.
[20] Nisha, J. Gut, P.J. Rosenthal, V. Kumar, Kumar, β-amino-alcohol tethered 4-aminoquinoline-isatin conjugates: Synthesis and antimalarial evaluation, Eur. J. Med. Chem. 84 (2014) 566–573.
[21] Z.H. Chohan, H. Pervez, A. Rauf, K.M. Khan, C.T. Supuran, Isatin-derived antibacterial and antifungal compounds and their transition metal complexes, J. Enzyme Inhib. Med. Chem. 19 (5) (2004) 417–423.
[22] S.K. Sridhar, M. Saravanan, A. Ramesh, Synthesis and antibacterial screening of hydrazones, Schiff and Mannich bases of isatin derivatives, Eur. J. Med. Chem. 36 (7-8) (2001) 615–625.
[23] J.M. Hwang, T. Oh, T. Kaneko, A.M. Upton, S.G. Franzblau, Z. Ma, S.-N. Cho, P. Kim, Design, synthesis, and structure–activity relationship studies of tryptanthrins as anti-tubercular agents, J. Nat. Prod. 76 (2013) 354–367.
[24] L.-S. Feng, M.-L. Liu, B.o. Wang, Y. Chai, X.-Q. Hao, S. Meng, H.-Y. Guo, Synthesis and in vitro anti-mycobacterial activity of balofloxacin ethylene isatin derivatives, Eur. J. Med. Chem. 45 (8) (2010) 3407–3412.
[25] L.-S. Feng, M.-L. Liu, S. Zhang, Y. Chai, B.o. Wang, Y.-B. Zhang, K. Lv, Y. Guan, H.-Y. Guo, C.-L. Xiao, Synthesis and in vitro anti-mycobacterial activity of 8-OCH_3 ciprofloxacin methylene and ethylene isatin derivatives, Eur. J. Med. Chem. 46 (1) (2011) 341–348.
[26] D. Sriram, A. Aubry, P. Yogeeswari, L.M. Fisher, Gatifloxacin derivatives: Synthesis, anti-mycobacterial activities, and inhibition of Mycobacterium tuberculosis DNA gyrase, Bioorg. Med. Chem. Lett. 16 (2006) 2982–2985.
[27] S.S. Karki, R. Hazare, S. Kumar, A. Saxena, A. Katiyar, Synthesis and antimicrobial activity of some 3-substituted-2-oxindole derivatives, Turk J. Pharm. Sci. 8 (2011) 169–178.
[28] T. Aboul-Fadl, M. Abdel-Hamid, A. Youssef, Schiff bases of indoline-2,3-dione (isatin) derivatives as efficient agents against resistant strains of Mycobacterium tuberculosis, Der Pharma Chem. 7 (2015) 217–225.
[29] M. Biava, G. Cesare Porretta, D. Deidda, R. Pompei, A. Tafi, F. Manetti, Importance of the thiomorpholine introduction in new pyrrole derivatives as anti-mycobacterial agents analogues of BM 212, Bioorg. Med. Chem. 11 (4) (2003) 515–520.
[30] M.R. Barbachyn, D.K. Hutchinson, S.J. Brickner, M.H. Cynamon, J.O. Kilburn, S. P. Klemens, S.E. Glickman, K.C. Grega, S.K. Hendges, D.S. Toops, C.W. Ford, G. E. Zurenko, Identification of a novel oxazolidinone (U-100480) with potent anti-mycobacterial activity, J. Med. Chem. 39 (3) (1996) 680–685.
[31] D. Sriram, P. Yogeeswari, K. Madhu, Synthesis and in vitro and in vivo anti-mycobacterial activity of isonicotinoyl hydrazones, Bioorg. Med. Chem. Lett. 15 (20) (2005) 4502–4505.
[32] Ş.G. Küçükgüzel, S. Rollas, I. Küçükgüzel, M. Kiraz, Synthesis and anti-mycobacterial activity of some coupling products from 4-aminobenzoic acid hydrazones, Eur. J. Med. Chem. 34 (12) (1999) 1093–1100.
[33] Global Alliance for TB drug development, Study to evaluate the safety, tolerability, pharmacokinetics of Sutezolid, https://clinicaltrials.gov/ct2/show/NCT03199313 (accessed July 22, 2020).
[34] H.M. Patel, M. Palkar, R. Karpoormath, Exploring MDR-TB inhibitory potential of 4-amino quinazolines as Mycobacterium tuberculosis N-acetylglucosamine-1-phosphate uridyltransferase (GlmU MTB) inhibitors, Chem. Biodiv. 17 (8) (2020), https://doi.org/10.1002/cbdv.v17.810.1002/cbdv.202000237.
[35] M.S. Shaikh, A.M. Kanhed, B. Chandrasekaran, M.B. Palkar, N. Agrawal, C. Lherbet, G.A. Hampannavar, R. Karpoormath, Discovery of novel N-methyl carbazole tethered rhodanine derivatives as direct inhibitors of Mycobacterium tuberculosis InhA, Bioorg. Med. Chem. Lett. 29 (16) (2019) 2338–2344.
[36] G.A. Hampannavar, R. Karpoormath, M.B. Palkar, M.S. Shaikh, B. Chandrasekaran, Dehydrozingerone inspired styryl hydrazine thiazole hybrids as promising class of anti-mycobacterial agents, ACS Med. Chem. Lett. 7 (7) (2016) 686–691.
[37] S.G. Shingade, S.B. Bari, U.B. Waghmare, Synthesis and antimicrobial activity of 5-chloroindoline-2, 3-dione derivatives, Med. Chem. Res. 21 (7) (2012) 1302–1312.
[38] K.M. Khan, M. Khan, M. Ali, M. Taha, S. Rasheed, S. Perveen, M.I. Choudhary, Synthesis of bis-Schiff bases of isatins and their antiglycation activity, Bioorg. Med. Chem. 17 (22) (2009) 7795–7801.
[39] W.M. Eldehna, A. Altoukhy, H. Mahrous, H.A. Abdel-Aziz, Design, synthesis and QSAR study of certain isatin-pyridine hybrids as potential anti-proliferative agents, Eur. J. Med. Chem. 90 (2015) 684–694.
[40] H.E. Dweedar, H. Mahrous, H.S. Ibrahim, H.A. Abdel-aziz, Analogue-based design, synthesis and biological evaluation of anticancer agents, Eur. J. Med. Chem. 78 (2014) 275–280.
[41] A. Zelmer, P. Carroll, N. Andreu, K. Hagens, J. Mahlo, N. Redinger, B.D. Robertson, S. Wiles, T.H. Ward, T. Parish, J. Ripoll, G.J. Bancroft, U.E. Schaible, A new in vivo model to test anti-tuberculosis drugs using fluorescence imaging, J. Antimicrob. Chemother. 67 (8) (2012) 1948–1960.
[42] J. Ollinger, M.A. Bailey, G.C. Moraski, A. Casey, S. Florio, T. Alling, M.J. Miller, T. Parish, P.C. Karakousis, A dual read-out assay to evaluate the potency of compounds active against Mycobacterium tuberculosis, PLoS ONE 8 (4) (2013) e60531, https://doi.org/10.1371/journal.pone.006053110.1371/journal.pone.0060531.g00110.1371/journal.pone.0060531.g00210.1371/journal.pone.0060531.g00310.1371/journal.pone.0060531.g00410.1371/journal.pone.0060531.g00510.1371/journal.pone.0060531.g00610.1371/journal.pone.0060531.t00110.1371/journal.pone.0060531.t002.
[43] Y.U. Cebici, H. Bayrak, Y. Sirin, Synthesis of novel Schiff bases and azol-β- lactam derivatives starting from morpholine and thiomorpholine and investigation of their anti-tubercular, antiurease activity, acethylcolinesterase inhibition effect and antioxidant capacity, Bioorg. Chem. 88 (2019), 102928.
[44] S.H. Cho, S. Warit, B. Wan, C.H. Hwang, G.F. Pauli, S.G. Franzblau, Low- oxygen-recovery assay for high-throughput screening of compounds against nonreplicating

Mycobacterium tuberculosis, Antimicrob. Agents Chemother. 51 (4) (2007) 1380–1385.
[45] N. Andreu, A. Zelmer, T. Fletcher, P.T. Elkington, T.H. Ward, J. Ripoll, T. Parish, G. J. Bancroft, U. Schaible, B.D. Robertson, S. Wiles, T.M. Doherty, Optimisation of bioluminescent reporters for use with mycobacteria, PLoS ONE 5 (5) (2010) e10777, https://doi.org/10.1371/journal.pone.0010777.
[46] M.F. Abo-Ashour, W.M. Eldehna, A. Nocentini, A. Bonardi, S. Bua, H.S. Ibrahim, M. M. Elaasser, V. Kryštof, R. Jorda, P. Gratteri, S.M. Abou-Seri, C.T. Supuran, 3-Hydrazinoisatin-based benzenesulfonamides as novel carbonic anhydrase inhibitors endowed with anticancer activity: Synthesis, in vitro biological evaluation and in silico insights, Eur. J. Med. Chem. 184 (2019), 111768.
[47] S.G. Franzblau, R.S. Witzig, J.C. McLaughlin, P. Torres, G. Madico, A. Hernandez, M.T. Degnan, M.B. Cook, V.K. Quenzer, R.M. Ferguson, R.H. Gilman, Rapid, low-technology MIC determination with clinical Mycobacterium tuberculosis isolates by using the microplate alamar blue assay, J. Clin. Microbiol. 36 (2) (1998) 362–366.
[48] Schrödinger-Maestro, Schrödinger Release, 2019-3.
[49] C. Balakumar, M. Ramesh, C.L. Tham, S.P. Khathi, F. Kozielski, C. Srinivasulu, G. A. Hampannavar, N. Sayyad, M.E. Soliman, R. Karpoormath, Ligand- and structure-based in silico studies to identify kinesin spindle protein (KSP) inhibitors as potential anticancer agents, J. Biomol. Struct. Dyn. 36 (14) (2018) 3687–3704.
[50] Y.H. Zhao, J. Le, M.H. Abraham, A. Hersey, P.J. Eddershaw, C.N. Luscombe, D. Boutina, G. Beck, B. Sherborne, I. Cooper, J.A. Platts, Evaluation of human intestinal absorption data and subsequent derivation of a quantitative structure – activity relationship (QSAR) with the Abraham descriptors, J. Pharm. Sci. 90 (6) (2001) 749–784.
[51] S.P. Khathi, B. Chandrasekaran, S. Karunanidhi, C.L. Tham, F. Kozielski, N. Sayyad, R. Karpoormath, Design and synthesis of novel thiadiazole-thiazolone hybrids as potential inhibitors of the human mitotic kinesin Eg5, Bioorg. Med. Chem. Lett. 28 (17) (2018) 2930–2938.
[52] S.K. Talapatra, C.L. Tham, P. Guglielmi, R. Cirilli, B. Chandrasekaran, R. Karpoormath, S. Carradori, F. Kozielski, Crystal structure of the Eg5-K858 complex and implications for structure-based design of thiadiazole-containing inhibitors, Eur. J. Med. Chem. 156 (2018) 641–651.
[53] R.J. Lambert, J. Pearson, Susceptibility testing: accurate and reproducible minimum inhibitory concentration (MIC) and non-inhibitory concentration (NIC) values, J. Appl. Microbiol. 88 (2000) 784–790.
[54] S. Release, Protein Preparation Wizard, Epik, Schrödinger, LLC, New York, NY, 2008.
[55] T.A. Halgren, R.B. Murphy, R.A. Friesner, H.S. Beard, L.L. Frye, W.T. Pollard, J. L. Banks, Glide: a new approach for rapid, accurate docking and scoring. 2. Enrichment factors in database screening, J. Med. Chem. 47 (7) (2004) 1750–1759, https://doi.org/10.1021/jm030644s.
[56] R.A. Friesner, J.L. Banks, R.B. Murphy, T.A. Halgren, J.J. Klicic, D.T. Mainz, M. P. Repasky, E.H. Knoll, M. Shelley, J.K. Perry, D.E. Shaw, P. Francis, P.S. Shenkin, Glide: a new approach for rapid, accurate docking and scoring. 1. Method and assessment of docking accuracy, J. Med. Chem. 47 (7) (2004) 1739–1749, https://doi.org/10.1021/jm0306430.
[57] B. Vijayakumar, S. Parasuraman, R. Raveendran, D. Velmurugan, Identification of natural inhibitors against angiotensin I converting enzyme for cardiac safety using induced fit docking and MM-GBSA studies, Pharmacogn Mag 10 (Suppl 3) (2014) S639–S644, https://doi.org/10.4103/0973-1296.139809.
[58] H.M. Patel, M. Shaikh, I. Ahmad, D. Lokwani, S.J. Surana, BREED based de novo hybridization approach: generating novel T790M/C797S-EGFR tyrosine kinase inhibitors to overcome the problem of mutation and resistance in non-small cell lung cancer (NSCLC) [published online ahead of print, J. Biomol. Struct. Dyn. 39 (8) (2021) 2838–2856, https://doi.org/10.1080/07391102.2020.1754918.
[59] K.A. Casalvieri, C.J. Matheson, D.S. Backos, P. Reigan, Molecular docking of substituted pteridinones and pyrimidines to the ATP-binding site of the N-terminal domain of RSK2 and associated MM/GBSA and molecular field datasets, Data Brief 29 (2020) 105347, https://doi.org/10.1016/j.dib.2020.105347.
[60] Desmond Molecular Dynamics System, D. E. Shaw Research, New York, NY, 2018-4. Maestro-Desmond Interoperability Tools, Schrödinger, New York, NY, 2018-4.
[61] H.M. Patel, I. Ahmad, R. Pawara, M. Shaikh, S.J. Surana, In silico search of triple mutant T790M/C797S allosteric inhibitors to conquer acquired resistance problem in non-small cell lung cancer (NSCLC): a combined approach of structure-based virtual screening and molecular dynamics simulation, J. Biomol. Struct. Dyn. (2020) 1–15, https://doi.org/10.1080/07391102.2020.1734092.
[62] Z. Jin, Y. Wang, X.-F. Yu, Q.-Q. Tan, S.-S. Liang, T. Li, H. Zhang, P.-C. Shaw, J. Wang, C. Hu, Structure-based virtual screening of influenza virus RNA polymerase inhibitors from natural compounds: Molecular dynamics simulation and MM-GBSA calculation, Comput. Biol. Chem. 85 (2020) 107241, https://doi.org/10.1016/j.compbiolchem.2020.107241.